

## **Online Appendix**

Using biological control data to understand host-pathogen  
dynamics

Mihaljevic *et al.*

## Contents

<b>1</b>	<b>Management Implications of Our Work</b>	<b>1</b>
<b>2</b>	<b>Observational data</b>	<b>2</b>
<b>3</b>	<b>Field transmission experiments</b>	<b>5</b>
3.1	Additional experimental details . . . . .	5
3.2	Fitting the SEIR model to the experimental data . . . . .	8
<b>4</b>	<b>Speed of kill experiment</b>	<b>11</b>
<b>5</b>	<b>Experimental estimate of the ratio parameter, <math>\rho</math></b>	<b>13</b>
<b>6</b>	<b>Effects of stochasticity in the model</b>	<b>13</b>
<b>7</b>	<b>Fitting Algorithm and Model Selection</b>	<b>16</b>
7.1	Line-search, Markov chain Monte Carlo (line-search MCMC) . . . . .	17
7.2	Likelihood calculation . . . . .	18
7.3	Conceptual Basis of WAIC . . . . .	20
7.4	Transmission Rates From the Best 2- $\bar{v}$ Model . . . . .	22
<b>8</b>	<b>Disease-density threshold</b>	<b>24</b>
<b>9</b>	<b>Marginal posteriors from 1-<math>\bar{v}</math> models</b>	<b>25</b>
<b>10</b>	<b>Marginal Posteriors For the 2-<math>\bar{v}</math> Models</b>	<b>34</b>
<b>11</b>	<b>Visual fits to the observational data for each of the 1-<math>\bar{v}</math> models.</b>	<b>40</b>
<b>12</b>	<b>Visual fits to the observational data for each of the 2-<math>\bar{v}</math> models.</b>	<b>44</b>
<b>13</b>	<b>JAGS model statement for fitting the transmission model to experimental data</b>	<b>48</b>



## 1 Management Implications of Our Work

1. Epidemiological models can be used to describe natural baculovirus epizootics, which lead  
3 to population crashes in Douglas-fir tussock moth (DFTM) populations. Managers are usually  
able to predict population crashes after 1-2 years of intense defoliation, but epidemiological  
models show that epizootics can decimate populations even before substantial defoliation occurs.
- 6 Infection rates often sharply increase when larvae reach the third or fourth instar and viral spread  
may therefore out pace defoliation. These findings suggest that additional consideration may be  
warranted prior to the decision to treat an area affected by a DFTM outbreak.
- 9 2. When the DFTM population is sufficiently large, very low initial infection rates can generate  
an epizootic strong enough to curtail defoliation. Even initial densities as low as 7 larvae/ $m^2$   
are sufficient for epizootics to occur. When assays of initial infection are conducted, 25% initial  
12 infection has historically been the threshold at which a decision to treat an area is made, while  
infection rates below 25% have been considered to be too low for meaningful epizootics to occur  
(Stelzer, 1979). Our work, however, shows that natural epizootics may occur even when initial  
15 infection rates are much lower, and so this threshold is far too conservative.
3. NPV spray programs are labor intensive and materials intensive. Comprehensive pre-  
season assays of infection rates may allow for more accurate prediction of baculovirus mortality  
18 rates, but such assays require considerable time and effort in the laboratory. When combined  
with the epidemiological modeling approach presented here, however, such laboratory efforts  
could result in significant savings of money and effort. This is because, in many cases, naturally  
21 occurring baculovirus epizootics will decimate DFTM populations, even in the absence of a spray  
program.
4. Detailed knowledge of epidemiological theory is not required to use the model, and we are  
24 therefore planning to develop a web-based application for managers that will allow prediction  
of epizootic dynamics. The data inputs required will be the host density and the initial infection  
rate. Host density can be obtained by standard cocoon or egg mass surveys, which are often

<sup>27</sup> carried out by forest health management personnel. The initial infection rate can be estimated by hatching out field-collected egg masses in the lab, to determine the fraction of larvae that hatch out infected. Managers usually estimate the fraction infected as well, but our results indicate that  
<sup>30</sup> more intensive searches for low initial infection rates may be necessary.

## 2 Observational data

In two cases, one the work of Otvos et al. (1987) in the Kamloops Forest District of British Columbia, and one the work of a co-author (C.J.M.) in the Methow Valley of Washington State, data were collected both from sprayed treatment plots (Otvos et al.: 4 sites; C.J.M.: 1 site), and control sites (Otvos et al.: 3 sites; C.J.M.: 2 sites, reported in Polivka et al. 2012). One of us (K.M.P.) also collected data from two naturally occurring epizootics, one in the Lovell Valley (Benewah Co.), Idaho, and one in Cheyenne Mountain State Park in Colorado (table A1).

Initial host density in our observation sites was measured using one of three methods, depending on the site. The first two methods consisted of standardized cocoon or egg mass surveys in the fall or spring preceding the insect collection, respectively (Mason et al., 1993). Cocoon surveys were conducted for the 2010 Washington sites, while an egg mass survey was conducted for the Idaho site. In these surveys, 25 trees were randomly selected across a 0.8 to 2.0 *ha* area, and the number of cocoons or egg masses on the underside of three 45 *cm* branch tips in the lower crown of each tree was counted (Mason et al., 1993). Because the pupae in the cocoons give rise to adult moths, we inferred the density of larvae resulting from cocoons by multiplying cocoon density by 0.5 to approximate the density of emerging females, and we inferred the initial larval density by multiplying by 145, the average number of larvae that hatch per egg mass (Mason et al., 1977). For the egg-mass survey data, we used the same calculation, except that of course we did not need to multiply by 0.5 to account for the fraction of pupae that produce females.

The third method consisted of larval surveys in the early spring preceding virus treatment, and was used by Otvos et al. (1987). In these surveys, 90 45 *cm* branch samples were taken from

Site	Location	Year	Initial Host Density (Larvae · $m^{-2}$ )
C1	Washington	2010	7.20
C2	British Columbia	1987	44.35
C3	Colorado <sup>a</sup>	2015	47.85
C4	British Columbia	1987	112.09
C5	Idaho	2010	126.08
C6	Washington	2010	149.00
C7	British Columbia	1987	165.39
T1	Washington	2010	8.99
T2	British Columbia	1987	34.27
T3	British Columbia	1987	124.08
T4	British Columbia	1987	172.65
T5	British Columbia	1987	232.03

Table A1: Labels and characteristics of sites used for the observational data set. C1, C2, and so on indicate unsprayed control sites, while T1, T2 and so on indicate sprayed sites. <sup>a</sup>The initial host density for the Colorado site was estimated from the data (see *Methods* section and Supplementary Materials).

45 trees at each site. The foliage area was estimated for each branch, and larvae were counted to yield larval density per  $m^2$ , which was then averaged across branches (Otvos et al., 1987). We  
54 did not have an estimate of initial host density for the 2015 control site in Colorado, and so for that site, we estimated the initial larval density along with the epidemiological parameters.

In some control sites, several weeks passed before sampling began, or before any infections  
57 were detected. In these cases, we adjusted the initial host density to account for non-disease mortality, due for example to predation or dessication, before the epizootic began. To simplify the problem, we assumed that this mortality rate was constant, and we estimated it using data

60 from Mason and Torgersen (1983) on larval survivorship in two tussock moth populations. We  
fit a simple model of density-independent mortality to these data, using a binomial likelihood,  
which gives a log-likelihood score of:

$$-\sum_t (N(0) - N(t)) \log(1 - e^{-bt}) + N(t) \log(e^{-bt}). \quad (\text{A1})$$

63 Here, the initial population size  $N(0) = 150$ , while  $N(t)$  is the population size at  $t$  days post  
hatching. To estimate the mortality rate  $b$ , we used the one-dimensional nonlinear fitting function  
`optimize()` in the R statistical language. The best-fit mortality rate is  $b = 0.037$ . As fig. A1  
66 shows, the model provides a reasonable fit to the data, suggesting that the assumption of constant  
mortality is reasonable. Also, the model provided a good fit to data from both branches on which  
emigration was allowed, and on branches from which emigration was prevented, suggesting that  
69 mortality was mostly due to predation rather than to emigration. We used this estimate of  $b$  to  
adjust the initial susceptible host density in epizootics for which the virus infection rate was zero  
for 2 or more weeks early in the larval period.

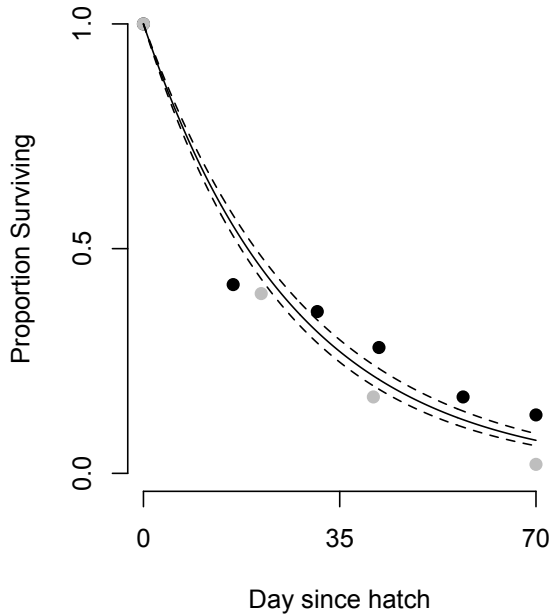


Figure A1: Fit of a density-independent mortality model to data from Mason and Torgersen (1983)'s fig 2. The black dots are data from experimental populations that were exposed to natural mortality factors, including predators, and for which emigration was allowed. Gray dots are data from adjacent populations for which emigration was prevented using cages that allowed access by small predators. The solid lines represent the maximum likelihood estimate of the decay function, while the dashed lines represent bootstrapped 95% confidence bounds.

72

### 3 Field transmission experiments

#### 3.1 Additional experimental details

Because the transmission rate,  $\nu$ , represents the overall infection risk per unit time, it encompasses both the probability of exposure and the probability of infection given exposure. Because  $\nu$  thus allows for host behavior and host-tree foliage effects, it is best measured using experiments

in which larvae feed freely on virus-contaminated foliage, preferably in the field. Previous work  
78 has shown that, by using the correct protocol, it is possible to carry out field-transmission experiments that are highly repeatable (Dwyer, 1991; Dwyer et al., 1997; Fleming-Davies et al., 2015).  
Following these protocols, we first reared uninfected tussock moth larvae in the laboratory from  
81 field-collected egg masses, which had been collected from an early-stage outbreak in Cheyenne Mountain State Park in Colorado in 2014. We used hatchling larvae as infected hosts in our experimental epizootics, because the most important round of transmission occurs when third  
84 and fourth instar larvae are infected by first instar cadavers. To deactivate any virus particles on the surface of the eggs, we submerged the egg masses in 5% formalin for 90 minutes prior to incubation (Dwyer and Elkinton, 1995). To cause infection, we placed the hatchlings on artificial  
87 diet contaminated with the respective viral isolate. A small pilot study allowed us to determine the viral dose that results in ~95% of larvae becoming infected (Mihaljevic et al., *unpublished data*).

90 Infected larvae were reared at 26 °C in the laboratory for five days to ensure that they were infected. Uninfected larvae can be easily identified and removed because they have molted to the second instar by this time (Fuller et al., 2012). Infected larvae were then placed on mesh-bag-  
93 enclosed Douglas-fir branches in the field at two densities: 10 and 40 larvae per ~0.5 m<sup>2</sup> branch. We then allowed the infected larvae to disperse on the foliage and die, which takes roughly 5 days. On the fifth day, we added 20 uninfected larvae, which we had reared in the lab to the  
96 fourth instar, the stage at which most transmission occurs in the wild (Dwyer et al., 1997). We also established seven control replicates by adding 20 uninfected fourth instar larvae to bagged branches without infected larvae.

99 Because a larval insect's susceptibility to a baculovirus can vary in a complex way within an instar (Grove and Hoover, 2007), we developmentally synchronized the fourth instars that we used as uninfected larvae. When a larva is ready to molt to the next instar, its head capsule  
102 slips forward, making it easy to identify larvae that are close to the end of an instar. To generate synchronized fourth instars for our experiment, we therefore collected third instars with slipped

head capsules, and we held them at 4°C, halting development, until we had enough larvae to  
105 begin the experiment. We then moved all the larvae to 26°C until they had molted to the fourth  
instar, which occurred within 48 hours. This protocol produces larvae that have all reached the  
fourth instar within a relatively short period. The similarity in infection risk among these larvae  
108 eliminates most extraneous variability, leaving only the binomial variation that is expected in an  
infection experiment (Elder et al., 2008).

Our experimental treatments thus consisted of 2 viral densities (10, 40), crossed with 3 viral  
111 isolates (TMB-1, WA, NM), for a total of 6 treatments, each replicated 14 times, with 7 control bags  
(viral density = 0). The experiment therefore included 91 total mesh bags and 1,820 uninfected,  
fourth instar larvae. We allowed the initially uninfected larvae to feed on foliage for 7 days, and  
114 then we removed the branches from the trees and brought them into the laboratory. Larvae from  
the branches were then reared individually in 2 ounce (59 ml) cups partially filled with artificial  
tussock moth diet. To determine if larvae had died because of the virus, we examined smears  
117 from dead larvae under a light microscope at 400× to determine if occlusion bodies were present.

After the 7 day experimental period, we photographed each branch, and we used ImageJ  
(Schindelin et al., 2015) to estimate the 2-dimensional surface area of foliage for each branch. The  
120 number of cadavers divided by the estimated foliage area per branch then served as an estimate  
of infectious-cadaver density. The density units were thus the same as in the epizootic data.

As described in the main text, we used three baculovirus isolates in this experiment, two nat-  
123 urally occurring isolates (WA and NM), and TMB-1, which is used in the spray formulation. The  
two naturally occurring isolates came from individual infectious cadavers that were originally  
collected as live larvae in the field. One of these isolates was collected from a control plot in the  
126 2010 spray program in Washington, while the other was collected near Los Alamos, New Mexico  
in 2014. Transmission electron microscopy showed that all three isolates were the multicapsid  
form of the virus, known as “*OpMNPV*” (Hughes and Addison, 1970).

129 As part of this experiment, we attempted to measure the decay rate  $\mu$  of infectious cadavers on  
foliage, by allowing some cadavers to be exposed to sunlight outside of the mesh bags for 3 days.

3 days, however, proved to be too short a period for us to detect meaningful decay of the virus,  
 132 and we therefore do not report these results in detail. One of us (G.D.) was similarly unsuccessful  
 at estimating the decay rate when using exposure periods of 1, 4, 13, and 32 days (Dwyer, 1992).  
 It may therefore be that the decay rate of the virus is very low, as implied by the posterior median  
 135 of the decay rate for the models with experiment-based priors on the transmission rates (table  
 A3).

### 3.2 Fitting the SEIR model to the experimental data

Experimentally manipulating the initial density of cadavers,  $P_0$ , allowed us to estimate the average transmission rate  $\bar{v}$  and the variability in transmission rate  $C$  for each virus isolate, as follows. Viral breakdown was effectively zero (Fuller et al., 2012), and the experiment was short enough that none of the initially uninfected larvae died of the virus during the experiment. Because the infectious cadaver density was thus held constant, we can set  $dP/dt = 0$ , which in turn allows us to simplify the SEIR model so that we can solve for the fraction of infected larvae,  $i$ , on each branch (Dwyer et al., 1997). When we compare the model to the data in the main text, we use a negative log-transformed version of this equation, as follows:

$$-\log(1 - i) = \frac{1}{C^2} \log(1 + C^2 \bar{v} P_0 \hat{t} \rho) \quad (\text{A2})$$

138 Here,  $\hat{t}$  is the time larvae were exposed to virus on foliage, which was 7 days. The ratio parameter,  
 $\rho$ , is included because an implicit assumption of the SEIR model is that all larvae are in the fourth  
 instar, but the infectious cadavers in our experiment were in the first instar. The parameter  $\rho$   
 141 therefore scales the transmission rate so that it is expressed in terms of fourth-instar cadavers.  
 Because we had estimated  $\rho$  from another experiment, we included an experimentally-derived  
 prior on  $\rho$ .

We fit equation A2 to the data from the field transmission experiment to estimate  $\bar{v}$  and  $C$  for each virus isolate, and to estimate a marginal posterior for ratio,  $\rho$ . We explicitly tested for the effect of host heterogeneity on transmission by also fitting a simpler, nested model, which

assumes  $C \equiv 0$ :

$$-\log(1 - i) = \nu P_0 \hat{\rho}. \quad (\text{A3})$$

We used the Bayesian inference software, *JAGS* (<http://mcmc-jags.sourceforge.net/>) via the *rjags* package in R with vague priors for  $\bar{\nu}$  and  $C$ , and an experimentally-derived prior for ratio,  $\rho$ . To avoid biases in the parameter estimates, we explicitly allowed for error in the cadaver densities  $P_0$  in the statistical model. We then compared the full and nested models using WAIC (see below for the formal definition of WAIC). Example code for the fitting routine for this model is provided at the end of this document.

To use the results of this analysis in fitting the SEIR model to the data, we constructed log-normal prior probability distributions for transmission  $\bar{\nu}$ , heterogeneity  $C$ , and ratio  $\rho$ , from the marginal posterior samples generated from fitting the simplified SEIR model (eq. A2) to the experimental data. On a log scale, the marginal posterior samples were well described by normal distributions, and so we constructed priors by calculating sample means and standard deviations from the posterior marginals. We expressed transmission heterogeneity  $C$  in terms of the parameter  $k = 1/C^2$ , which has a distribution that is more nearly normal on a log scale. We thus used the following informative prior probability distributions:  $\bar{\nu} \sim LN(-4.82, 0.59)$ ,  $k \sim LN(-0.094, 0.75)$ ,  $\rho \sim LN(-3.39, 0.50)$ , where *LN* represents a log-normal distributions. For  $k$  and  $\rho$ , we inflated the prior variance slightly to improve chain mixing, but the effects were minimal.

Dessication is a common source of natural mortality in Douglas-fir tussock moth populations (Mason and Torgersen, 1983), and so seven of our 119 experimental branches had 100% mortality due to dessication. Because the mesh bags can elevate temperatures (Páez et al., 2017), we excluded these branches from our analyses. For the other branches, we similarly excluded dessicated larvae, which were unlikely to have become infected, and could only be autopsied with extreme difficulty. The estimated 2-dimensional area of foliage per replicate branch ranged from 0.09 to 0.28  $m^2$  (mean = 0.15). After correcting for this variability, the cadaver density for the low density treatment (10 cadavers per branch) ranged from 38.49 to 112.58 cadavers  $\cdot m^{-2}$  foliage

(mean = 70.58), and the high density treatment (40 cadavers per branch) ranged from 142.38 to 426.98 cadavers  $\cdot m^{-2}$  foliage (mean = 254.41).

Model Type	WA Isolate	NM Isolate	TMB-1	Overall
$C > 0$	175.53	<b>179.48</b>	<b>165.06</b>	<b>520.07</b>
$C = 0,$	174.28	199.11	168.45	541.84

Table A2: Model selection for the transmission experiment. The bold-faced WAIC scores highlight the best model, based on  $\Delta\text{WAIC} > 3$ .

<sup>171</sup> As Table A2 shows, for the WA data, the fit of the model with no heterogeneity ( $C = 0$ ) is indistinguishable from the fit of the model with  $C > 0$ . Over all 3 isolates, however, the model with  $C > 0$  provides a better fit.

## 4 Speed of kill experiment

DFTM egg masses were collected from sites C1 and T1 (table A1), sterilized, and reared to the fourth instar following the same protocols as the uninfected larvae in the field transmission experiment. Larvae were then exposed to the TMB-1 isolate by placing them on Douglas-fir seedlings in the greenhouse, at a temperature of 30 °C. To apply the virus to the foliage, we prepared a solution of TMB-1 (Lot no. 4 USDA Forest Service, Corvallis, Oregon) at a concentration of 0.018g ·l<sup>-1</sup>, equal to the concentration used in large microbial control projects (R. Magelssen, pers. comm.). We then sprayed the foliage with 4.5 mL, a quantity sufficient to cover all the foliage on the small trees that we used.

We allowed larvae to feed on the foliage for 7 days and then we transferred them individually to 2 oz cups with artificial diet. Larvae were then incubated at 27 °C and monitored daily for mortality. Larvae that died before pupation were autopsied to confirm virus death.

In the SEIR model, hosts proceed through several exposed classes, leading to a gamma-distributed speed of kill (see main text). To estimate the death rate parameter  $1/\delta$ , we therefore used Bayesian methods to fit the following gamma distribution to the speed of kill data;

$$f(x; \alpha, \beta) = \frac{\beta^\alpha x^{\alpha-1} e^{-\beta x}}{\Gamma(\alpha)} \quad (\text{A4})$$

In terms of the parameters  $\alpha$  and  $\beta$ , as well as the parameters  $m$  and  $\delta$  of the SEIR model, the mean of this distribution is:  $E[X] = \frac{\alpha}{\beta} = \frac{1}{\delta}$  and the variance is:  $\text{Var}[X] = \frac{\alpha}{\beta^2} = \frac{1}{m\delta^2}$ . Thus, by estimating  $\alpha$  and  $\beta$  from our speed of kill data, we were able to estimate the death rate parameter  $\delta$  in our epidemiological model.

We fit the gamma distribution in JAGS (<http://mcmc-jags.sourceforge.net/>) using flat priors for  $\alpha$  and  $\beta$ , three MCMC chains, an adaptation period of 10,000 iterations, and 50,000 sampling iterations, thinning by 50, for a total of 1000 samples from the posterior. The resulting distribution explains most of the variation in the data (fig. A2). From the posterior distribution of the parameters, the mean  $\alpha = 28.84$ , with variance = 42.6, while the mean  $\beta = 1.9$ , with variance =

195 0.2. Given the relationship between these parameters and  $\delta$ , our posterior mean  $\delta = 0.067$ , so  
that the speed of kill is approximately 15 days.

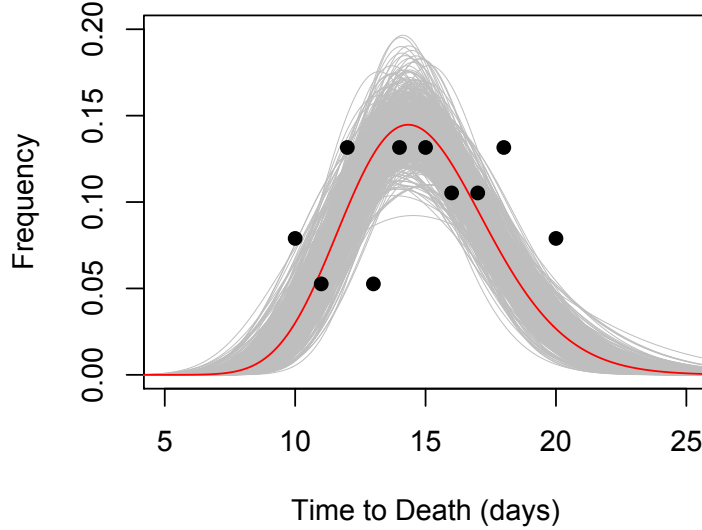


Figure A2: A comparison of the fitted gamma distribution to the speed of kill data. The black points represent the data, the red line represents the model's prediction based on the median values of the parameters, and the gray lines represent a set of model predictions using parameters drawn randomly from the joint posterior.

By allowing larvae to feed freely on virus-contaminated foliage, we attempted to ensure that  
198 the doses that larvae consumed were similar to the doses that they consume in nature. A possible  
downside to this approach, however, is that larvae may have became infected over several days,  
whereas in laboratory experiments, larvae typically become infected over a few hours (Dwyer  
201 et al., 2005). Possibly for this reason, the variance in the speed of kill was substantially larger than  
it was in a previous laboratory experiment (Dwyer, 1991), while nevertheless being extremely  
small compared to the mean (variance:  $4.4 \times 10^{-6}$ ). The experimental data therefore imply a  
204 value of  $m = 29$  (range 10-50), but because of the near-zero variance in previous work, in our

fitting routine, we set  $m = 200$ . In fact, for values of  $m$  much greater than 10, the variance in the speed of kill is very slight, so using  $m = 29$  probably would have given similar results.

## 207 5 Experimental estimate of the ratio parameter, $\rho$

To estimate the ratio parameter  $\rho$ , we infected 40 first instars and 20 fourth instars by exposing them to virus-contaminated diet in the lab, and then estimating the number of viral occlusion bodies (OBs) that were produced by each larva. We randomly assigned one of our three virus isolates to each larva, but to allow for variation across isolates, we pooled the data to produce an overall estimate of  $\rho$ . After exposure, larvae were reared individually at 26°C in 2oz cups until death, and then stored at -20°C in individual micro-centrifuge tubes. Thawed larvae were later vortexed in 5 mL of dH<sub>2</sub>O in the micro-centrifuge tubes, and then filtered through cheesecloth into a 50 mL centrifuge tube. After we added an additional 25 mL DI water to the tube, we centrifuged the solution for 10 minutes at 5000 g to pellet the virus. The supernatant was then poured off and the viral pellet was re-suspended in 10 mL of DI water. We vortexed the solution for 3 minutes and counted OBs using a hemocytometer. We calculated an average density of OB/ $\mu$ L from two replicate counts of 10  $\mu$ L aliquots of the virus isolate.

Viral densities ranged from 50 to 2150 OBs/ $\mu$ L for first instars, with a mean of 340, and from 1575 to 9775 OBs/ $\mu$ L for fourth instars, with a mean of 4832. Based on 1000 bootstraps of these data, we used the following log-normal prior distribution for  $\rho$  in the field experiment:  $\rho \sim LN(-2.77, 0.83)$ .

## 6 Effects of stochasticity in the model

In our model, the stochastic variation in transmission rates varied among sites, such that larger variation  $\sigma$  increased the effective transmission rate over the course of the epizootic. Increased stochasticity thus led to more severe epizootics than expected from a deterministic model with the same parameters (fig. A3).

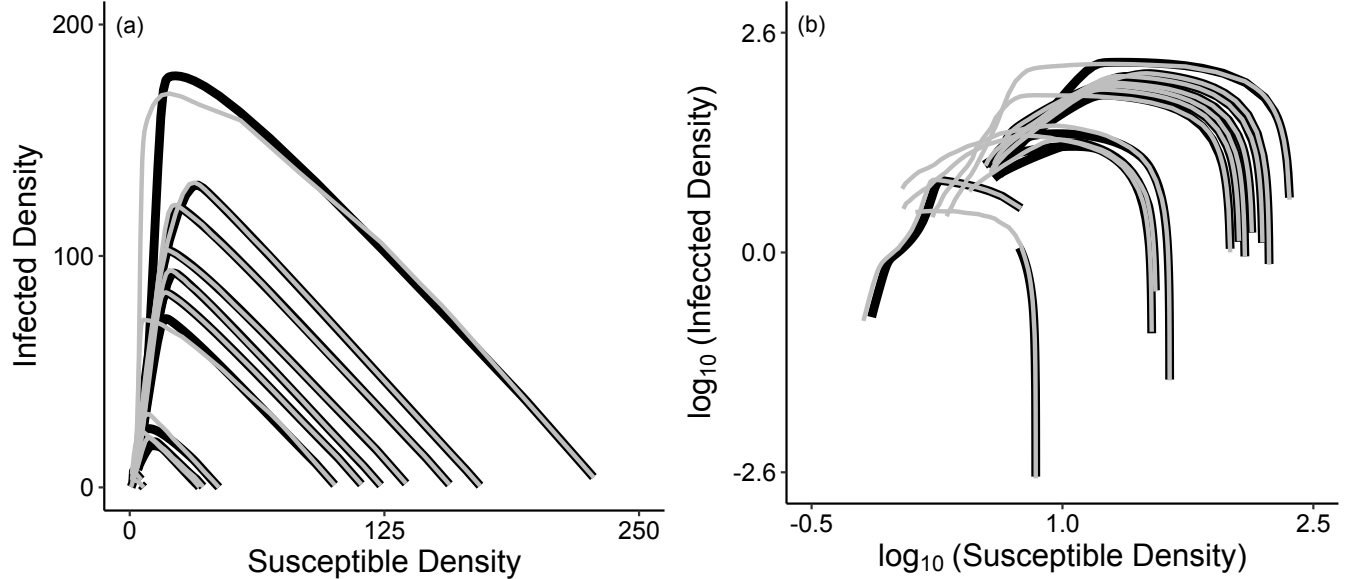


Figure A3: (a) Simulated phase portraits for our model, using initial conditions estimated from each of our twelve epizootics. The solid black lines represent trajectories from a deterministic version of the SEIR model, while the gray lines represent median trajectories over 500 realizations of the stochastic model, with time proceeding from right to left. The infected density in the model is measured as the sum of the densities in the exposed classes,  $\sum E_m$ . (b) Same as (a) but with log-transformed densities to illustrate more clearly that stochasticity leads to more severe epizootics.

To explain this effect, here we show that the mean transmission rate is always higher for the stochastic model. First, for the stochastic model, the average transmission rate  $E[\bar{v}]$  can be  
<sup>231</sup> expressed as:

$$E[v_t] = E[e^{\epsilon_t} \bar{v}] = \bar{v} E[e^{\epsilon_t}]. \quad (\text{A5})$$

The rightmost expectation can be calculated according to,

$$E[e^{\epsilon_t}] = \int e^{\epsilon_t} dP(\epsilon_t). \quad (\text{A6})$$

In practice, we specify that the distribution of the  $\epsilon_t$ 's is normal, and so by Jensen's inequality we

<sup>234</sup> have;

$$\int_{-\infty}^{\infty} e^{\epsilon_t} dp(\epsilon_t) = \int_{-\infty}^{\infty} e^x \frac{1}{\sqrt{2\pi\sigma^2}} e^{-\frac{x^2}{2\sigma^2}} dx > 1. \quad (\text{A7})$$

We therefore have that,

$$E[\nu] = \bar{\nu} E[e^{\epsilon_t}] > \bar{\nu}. \quad (\text{A8})$$

In other words, the expected transmission rate of the stochastic model is always higher than the

<sup>237</sup> (constant) transmission rate of the deterministic model.

Interestingly, our estimates of the stochasticity term  $\sigma$  vary in a consistent way with initial host

density. As fig. A4 shows, the estimated values of  $\sigma$  tended to be higher in plots with lower initial

<sup>240</sup> host densities, especially for control plots (fig. A4), and this trend is consistent across model types

(see *Marginal Posterior* section, below, for parameter estimates across model types). This result

suggests that what we are attributing to weather stochasticity may instead be stochasticity due to

<sup>243</sup> the chance events that befall individuals, known as “demographic stochasticity” (Bolker, 2008).

In our case, transmission can be affected by behavioral decision-making and individual variation

in exposure risk (Parker et al., 2010), either of which may be subject to chance at the individual

<sup>246</sup> level. Because demographic stochasticity has stronger effects in smaller populations, the higher

values of  $\sigma$  that we estimated in lower-density control plots may reflect demographic stochasticity.

In sprayed plots in contrast, demographic stochasticity may have had weaker effects because the

<sup>249</sup> initial inundation of virus may have homogenized infection risk across space relative to the

natural situation in which the virus is clumped into cadavers (D’Amico et al., 2005; Eakin et al.,

2015). The spray may therefore have reduced or eliminated the effects of individual variation in

<sup>252</sup> behavior early in the epizootic.

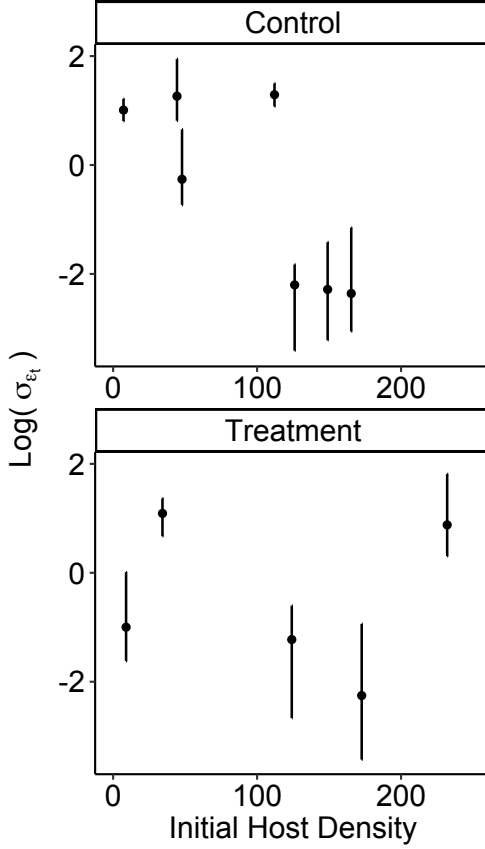


Figure A4: Relationship between stochastic transmission and initial host density for our 12 epizootics, separated into control and sprayed treatment plots. Error bars are 95% credible intervals.

## 7 Fitting Algorithm and Model Selection

Here we describe the algorithm that we used to fit our SEIR model to the epizootic data, and  
255 the details of our model selection approach. The algorithm that we used is known as “line search-MCMC”. Using line-search MCMC required that we carry out 3 steps, which can be  
briefly summarized as follows. First, we conducted a Bayesian line search through the multi-  
258 dimensional parameter space of the model, with multiple random re-starts of the line searches.  
Second, we performed principle components analysis (PCA) on the line-search results, in order  
to construct proposals for MCMC. We then used these proposals to implement an MCMC routine

261 to sample from the posterior distribution of the model, and thus to fit the model to the epizootic  
262 data. The first and third steps required that we calculate model likelihood scores by averaging  
263 across the likelihoods of many model realizations, effectively integrating out the stochasticity  
264 across realizations. Here we explain these steps in more detail. All methods were executed using  
custom code in the C programming language (Kernighan and Ritchie, 2006).

## 7.1 *Line-search, Markov chain Monte Carlo (line-search MCMC)*

267 The line-search MCMC method was first proposed by Kennedy et al. (2014) to adapt MCMC  
so that it takes advantages of developments in high performance computing, and to improve  
MCMC performance through automated proposal construction. Following the algorithm, we  
270 began with a line-search step in which we iteratively swept through parameter space, one pa-  
rameter at a time, calculating the posterior probability of each parameter set. Each line search  
swept through the parameter space many times, resulting in a “best” parameter set for each  
273 search. Line searches, however, generally get stuck at local maxima, or on ridges of the posterior  
probability surface. We therefore ran 2000 independent line-searches, with each started by ran-  
domizing the order of parameters in the search and the initial position in parameter space. Each  
276 search then produced a best parameter set, by maximizing the posterior probability.

Next, we used the top 5% of these 2000 parameter sets to construct automated proposal  
distributions for an MCMC routine. When MCMC is used to fit nonlinear models with more  
279 than a few parameters, correlations between parameters commonly disrupt the performance of  
the MCMC algorithm, by creating ridges on the surface of the posterior probability. To overcome  
this problem, we followed the line search-MCMC algorithm by using the top 5% of the 2000  
282 parameter sets from the line searches, as ordered by decreasing posterior probability, in a PCA.  
We then used the PCA results to generate proposals for MCMC.

To explain how the PCA results were used, we note first that, in a standard Metropolis-  
285 Hastings MCMC algorithm, a random value of a single parameter is drawn from a proposal  
distribution, a new likelihood is calculated for the new parameter set, and then a decision is

made to keep or reject the newly proposed parameter value. Following line search-MCMC, we  
 288 instead drew a parameter in PCA space, and then we back-calculated to produce a new full set of  
 model parameter values on the original, non-PCA-transformed scale. In each MCMC iteration,  
 we therefore proposed a full, uncorrelated set of parameters, before calculating likelihoods. This  
 291 vastly improved the mixing of our MCMC chains.

We ran 10 independent MCMC chains for each of our  $1-\bar{v}$  and  $2-\bar{v}$  models for at least 30,000  
 iterations, thinning by 100 iterations. This took approximately one week of computing or “wall-  
 294 clock time” for each model. We tested for convergence via the Potential Scale Reduction Factor,  
 $\hat{R}$ , (Gelman et al., 2014), and we used visual diagnostics to assess overall mixing, and within-  
 and among-chain auto-correlations and parameter correlations. Our results are based on strong  
 297 convergence, except for models for which heterogeneity  $C = 0$ . As we describe in the main text,  
 the latter models fit the data very poorly, so it may be that there is no Bayesian algorithm that  
 will converge for those models.

## 300 7.2 *Likelihood calculation*

For each set of parameters in the line search and MCMC steps, calculating likelihood scores is  
 challenging for two reasons. First, our model is stochastic, so we were forced to integrate the  
 303 likelihood over many realizations of the stochastic process. Second, our field observations may  
 have had extra-binomial variation, so we estimated and corrected for over-dispersion.

Because the specific values of the daily stochasticity  $\epsilon_t$  are not of interest, we integrated over  
 realizations, which effectively integrated out the values of the  $\epsilon_t$ s. To do this, we calculated an  
 average likelihood, as follows:

$$\bar{L} = \int L(\epsilon_1, \epsilon_2, \dots, \epsilon_D) f(\epsilon_1, \epsilon_2, \dots, \epsilon_D) d\epsilon_1 d\epsilon_2 \dots d\epsilon_D \quad (\text{A9})$$

Here  $\bar{L}$  is the likelihood, and  $D$  is the number of days for which we drew  $\epsilon_t$  values. Here  
 306  $f(\epsilon_1, \epsilon_2, \dots, \epsilon_D)$  is the probability density of the  $\epsilon_t$ 's. Because the model is quite complicated,  
 it can only be integrated numerically, and as we have discussed, this numerical integration is

computationally expensive. Calculating the integral in equation (A9) using numerical integration  
 309 methods, such as numerical quadrature, is therefore impractical.

We therefore instead used Monte Carlo integration (Ross, 2002). The idea behind Monte  
 Carlo integration is that we draw values of the  $\epsilon_t$ 's, and then we calculate the average likelihood  
 312 according to,

$$\hat{L} = \frac{1}{R} \sum_{j=1}^R L(\epsilon_1^j, \epsilon_2^j \dots \epsilon_D^j), \quad (\text{A10})$$

where  $R$  is the number of realizations, and  $\epsilon_1^j$  is the value of  $\epsilon_1$  in the  $j$ th realization. According  
 to the weak law of large numbers (Ross, 2002), as  $R \rightarrow \infty$ ,  $\hat{L} \rightarrow \bar{L}$ .

315 For reducing computing time, however, it is crucial that  $\hat{L}$  approaches  $\bar{L}$  for a reasonably  
 small number of realizations, and for this purpose we used the MISER Monte-Carlo integration  
 algorithm. This algorithm uses recursive, stratified sampling to estimate the average likelihood  
 318 while minimizing the number of realizations. Briefly, the algorithm works as follows (the code  
 that we use is from the Gnu Scientific Library, but for a more complete explanation, see Press  
 et al. (1992)). As equation (A10) shows, in calculating an estimate of the average likelihood  $\hat{L}$ ,  
 321 we are sampling over a  $D$ -dimensional space. Within this space, it is likely that there are sub-  
 spaces within which the variance in  $\hat{L}$  is higher than in other sub-spaces. In estimating  $\hat{L}$  across  
 the entire space, it is more efficient to sample more frequently in sub-spaces within which the  
 324 variance in  $\hat{L}$  is proportionately higher. It is possible to demonstrate this proposition formally,  
 and it therefore forms the basis of the MISER algorithm.

Accordingly, given a quota of  $R$  realizations, the algorithm first devotes some fraction of  
 327 the realizations, in our case 0.1, to sampling uniformly across the entire space. Based on this  
 initial sample, the algorithm recursively divides the overall space into sub-spaces of high and  
 low variance. In using the remaining realizations, the algorithm then samples more intensively  
 330 in sub-spaces of high variance. The end result is an estimate of  $\hat{L}$  that minimizes the variance,  
 subject to the constraint of a limited number of realizations. This algorithm allowed us to use only  
 150 realizations per likelihood calculation, because initial trials made clear that larger numbers

<sup>333</sup> of realizations were unnecessary.

For each likelihood calculation, we compared the fraction of infected insects from a given field observation to the fraction infected as generated by the model, expressed as  $\frac{\sum E_m}{\sum E_m + S}$ . We then  
<sup>336</sup> summed the log-likelihoods of the observations across plots, assuming a beta-binomial likelihood function with parameters  $a = pe^\gamma$  and  $b = (1 - p)e^\gamma$ , where  $p$  is the model prediction of the fraction infected and  $\gamma$  is an inverse measure of the over-dispersion of the binomial variation in  
<sup>339</sup> the data. We estimated  $\gamma$  from the data, using a vague prior. As we will show, over-dispersion levels were moderate but not excessive.

### 7.3 Conceptual Basis of WAIC

<sup>342</sup> In any model selection procedure, a fundamental goal is to produce a model that will best predict future data (Konishi and Kitagawa, 2008). In a Bayesian context, the accuracy of the model predictions can be summarized by the posterior predictive density, the probability of future data  
<sup>345</sup> given current data (Gelman et al., 2014);

$$p(\tilde{D}|D) = \int p(\tilde{D}|\theta)p(\theta|D)d\theta. \quad (\text{A11})$$

Here  $\tilde{D}$  is future data,  $D$  is current data, and  $\theta$  is a vector of parameters. The predictive accuracy of the model  $p(\tilde{D}|D)$  is thus calculated in terms of the probability of future data given the  
<sup>348</sup> parameters  $p(\tilde{D}|\theta)$ , and in terms of the posterior distribution of the parameters  $p(\theta|D)$ . By definition we have not yet collected future data, so the ability of a model to predict future data must be approximated by the model's ability to predict existing data. The likelihood of current  
<sup>351</sup> data, however, often over-estimates the likelihood of future data, because fitting a model to a current data set can lead to under-estimates of the uncertainty in the model's predictions of future data (Konishi and Kitagawa, 2008). In WAIC in particular, this tendency to over-fit current  
<sup>354</sup> data is corrected for in terms of the variance of the posterior predictive density, which can be approximated by the variance of the posterior (Watanabe, 2009).

The WAIC is thus defined as (Gelman et al., 2014):

$$\text{WAIC} = \sum_{i=1}^n \log \left( \frac{1}{S} \sum_{s=1}^S p(D_i | \theta^s) \right) + \sum_{i=1}^n V_{s=1}^S \log p(D_i | \theta^s)$$

357 The first term in the WAIC,  $p(D_i | \theta^s)$ , is the probability of the data given the parameters, which is  
an approximation to the expected log predictive density, a goodness of fit term. WAIC averages  
over  $n$  data points, which in our case corresponds to our 12 epizootic time series, and over  
360  $S$  random draws from the joint posterior distribution of the parameters  $\theta$ . We also averaged  
over the stochasticity in the model output. The second term penalizes more complex models in  
terms of  $V_{s=1}^S$ , an approximation to the variance of the log predictive density, which inevitably  
363 increases with the number of parameters. The variance term is also averaged over the  $n$  plots  
and the  $S$  random draws, as well as over the stochasticity in the model output. More complex  
models may provide less parsimonious explanations for the data, and so are likely to do a poor  
366 job of predicting future data or out-of-sample data. WAIC is thus asymptotically equivalent to  
cross-validation (Gelman et al., 2014).

Exploratory simulations demonstrated that, when the number of draws of parameter sets  
369 from the posterior was more than about 500, further increases in the number of draws had  
only small effects on the WAIC score. In contrast, the number of realizations of the stochastic  
model had a strong effect on the WAIC score, apparently because the number of realizations  
372 has strong effects on the penalty term of the WAIC (fig. A5). Accordingly, for each model,  
we calculated WAIC scores based on 750 parameter sets drawn from the posteriors, and by  
estimating likelihoods ( $\hat{L}$ ) using 1000 realizations of each epizootic.

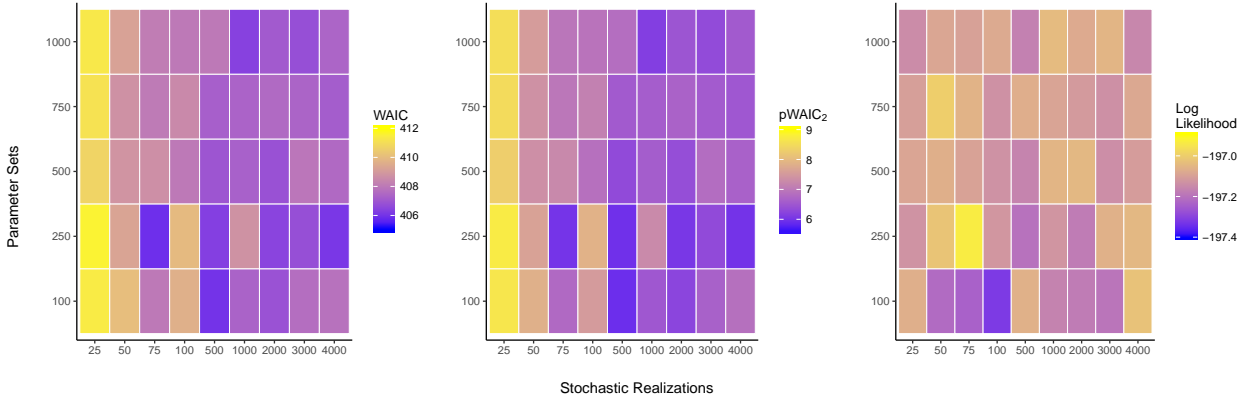


Figure A5: Effects of the number of parameter sets and the number of stochastic realizations on WAIC scores. Effects on the WAIC (left panel) are separated into effects on the penalty term (middle panel), and effects on the log likelihood (right panel). This simulation was carried out for the model that has an experiment-based prior on  $\delta$ , which has a WAIC score that is close to that of the best model.

375

#### 7.4 Transmission Rates From the Best 2- $\bar{v}$ Model

In the main text, we show that the best 2- $\bar{v}$  model, which has an informative prior for the death rate  $\delta$ , has almost the same WAIC score as the best 1- $\bar{v}$  model. As we described, however, the  
 378 estimates of the 2 separate transmission rates for the 2- $\bar{v}$  model are not meaningfully different. To show this, we made draws from the posteriors for each transmission rate, and we calculated differences between the two transmission rates for each draw. As we reported in the main text, the  
 381 95% credible interval (CI) for this distribution includes zero (CI: -0.13, 2.56; fig. A6), confirming that we cannot conclude that the two estimates are meaningfully different. There is, however, a trend in which spray virus transmission is slightly higher than naturally occurring transmission,  
 384 but this trend is likely due to the interaction between average transmission and stochasticity. That is, epizootics in unsprayed populations are better explained by parameter sets with lower average transmission and higher stochasticity in transmission. The trend towards higher transmission for  
 387 the sprayed virus therefore appears to be a statistical effect, rather than a biological effect.

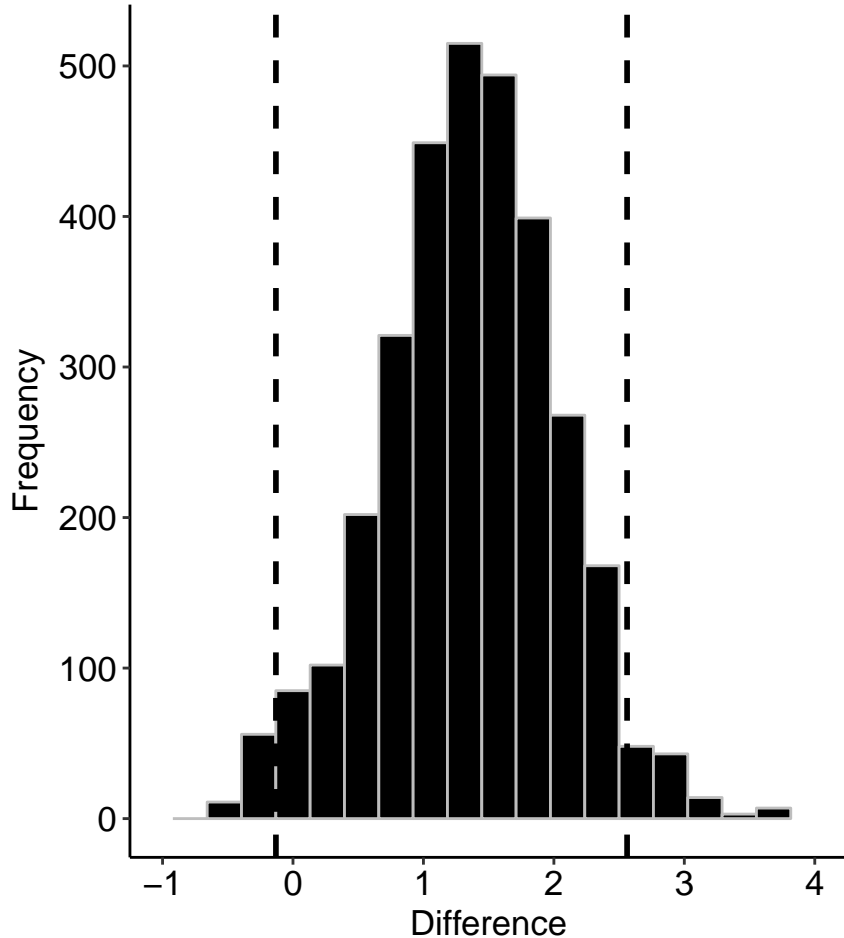


Figure A6: The difference between estimates of the log-transformed average transmission rates in the  $2-\bar{v}$  model for spray - control. These values were log-transformed before taking the difference. The 95% CI is between the vertical dashed lines, and includes 0.

Figure A7 shows the substantial overlap between the estimate of the average transmission rate for the best  $1-\bar{v}$  model ( $\bar{v}_1$ ), which has all uninformative priors, and for the two estimates  
 390 from the best  $2-\bar{v}$  model. The three estimates are thus not meaningfully different.

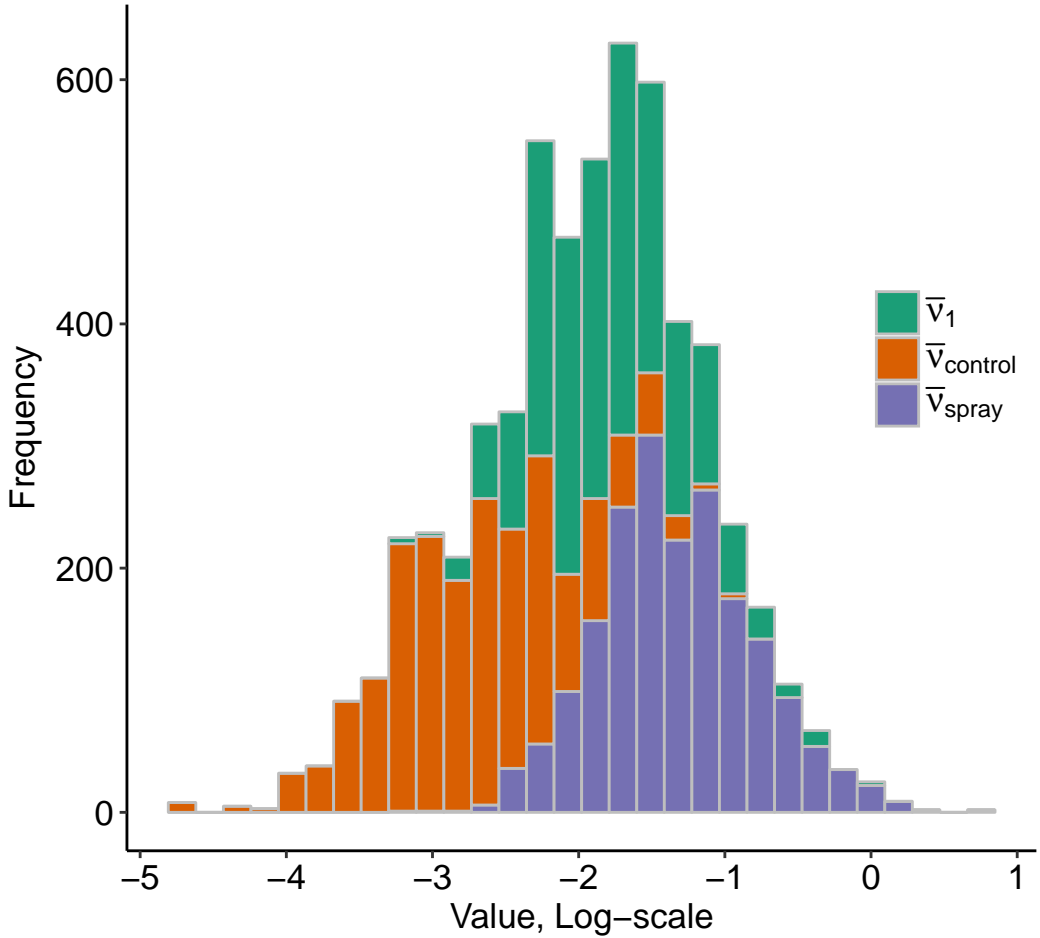


Figure A7: Stacked histograms showing the overlap between the three estimates of average transmission rate from the two best models.

## 8 Disease-density threshold

As described in the main text, our estimates of the disease-density thresholds differ only slightly  
 393 between  $1-\bar{v}$  models, yet the estimates of  $\bar{v}$  and  $\mu$  differ strongly between models. An obvious  
 question is therefore, why are the threshold values so similar? The answer seems to be that there  
 are correlations between the marginal posterior estimates of these two parameters both within  
 396 and between model types (fig. A8). For models with priors based on experiments, however, the  
 correlation between  $\bar{v}$  and  $\mu$  is weaker, making it easier to separately estimate  $\bar{v}$  and  $\mu$ . This effect

demonstrates another benefit of using experimental data to construct priors.

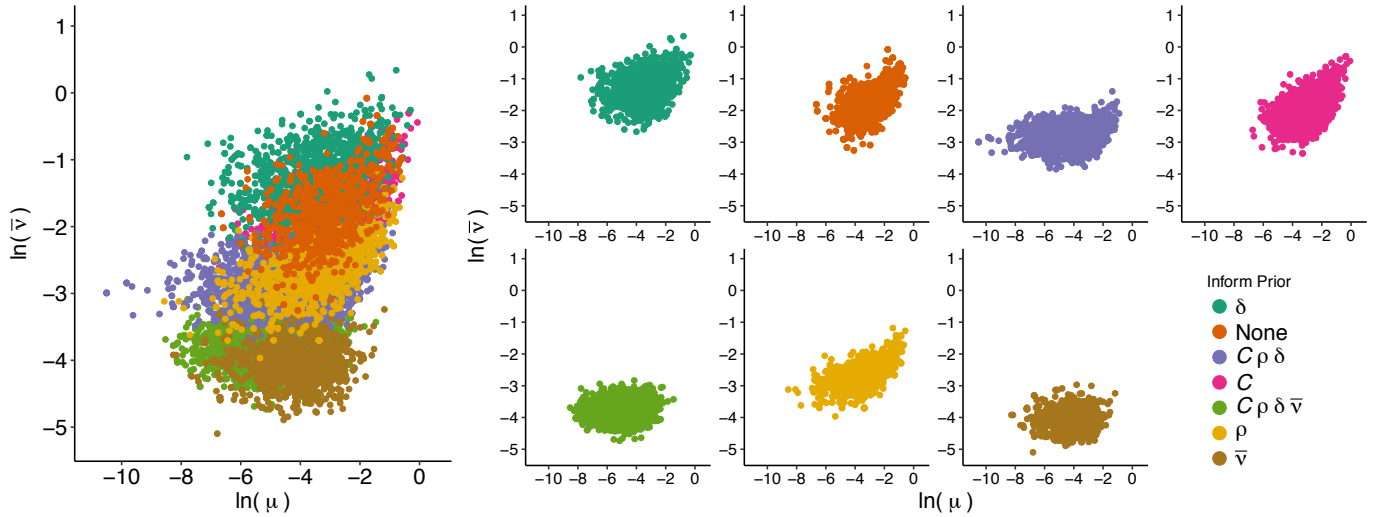


Figure A8: Relationship between marginal posterior samples of  $\ln(\bar{v})$  and  $\ln(\mu)$  from the  $1-\bar{v}$  models.

The panel on the left shows pooled samples from all models, while the panels on the right show samples for each model. The positive correlations between the two parameters lead to very similar estimates of the disease-density thresholds across models.

399

## 9 Marginal posteriors from $1-\bar{v}$ models

Here we present tables showing the marginal posterior parameter estimates derived from the  $1-\bar{v}$  models. In general, the median parameter estimates do not differ much between models,  
402 although there is modest variation in precision.

Table A3: Marginal posterior estimates of model parameters, where  $\gamma$  estimates the extra-binomial variation in fraction infected (see main text). Estimates are medians with 95% credible intervals. These are not on a log scale.

Parameter	Model (Informative Priors)	Estimate
-----------	-------------------------------	----------

	$\delta$	0.061 (0.055, 0.067)
	None	0.063 (0.056, 0.07)
	$C \rho \delta$	0.067 (0.059, 0.076)
$\delta$	$C$	0.063 (0.058, 0.07)
	$C \rho \delta \bar{\nu}$	0.077 (0.066, 0.087)
	$\rho$	0.065 (0.057, 0.076)
	$\bar{\nu}$	0.083 (0.064, 0.103)
<hr/>		
	$\delta$	1.360 (1.163, 1.588)
	None	1.275 (1.108, 1.530)
	$C \rho \delta$	1.150 (0.968, 1.337)
$C$	$C$	1.233 (1.024, 1.436)
	$C \rho \delta \bar{\nu}$	0.978 (0.813, 1.163)
	$\rho$	1.132 (0.963, 1.346)
	$\bar{\nu}$	0.836 (0.605, 1.086)
<hr/>		
	$\delta$	0.041 (0.001, 0.201)
	None	0.042 (0.001, 0.236)
	$C \rho \delta$	0.016 (0, 0.117)
$\mu$	$C$	0.053 (0.002, 0.221)
	$C \rho \delta \bar{\nu}$	0.007 (0, 0.037)
	$\rho$	0.031 (0.001, 0.255)
	$\bar{\nu}$	0.017 (0, 0.073)
<hr/>		
	$\delta$	0.277 (0.082, 0.545)
	None	0.166 (0.055, 0.377)
	$C \rho \delta$	0.059 (0.029, 0.101)
$\bar{\nu}$	$C$	0.136 (0.053, 0.267)
	$C \rho \delta \bar{\nu}$	0.024 (0.014, 0.037)

	$\rho$	0.07 (0.025, 0.14)
	$\bar{\nu}$	0.017 (0.008, 0.027)
	$\delta$	0.004 (0.001, 0.012)
	None	0.008 (0.002, 0.02)
	$C \rho \delta$	0.024 (0.01, 0.043)
$\rho$	$C$	0.01 (0.002, 0.023)
	$C \rho \delta \bar{\nu}$	0.047 (0.02, 0.083)
	$\rho$	0.023 (0.008, 0.044)
	$\bar{\nu}$	0.062 (0.025, 0.123)
	$\delta$	2.117 (1.801, 2.426)
	None	2.102 (1.831, 2.367)
	$C \rho \delta$	2.147 (1.864, 2.501)
$\gamma$	$C$	2.156 (1.886, 2.456)
	$C \rho \delta \bar{\nu}$	2.248 (1.995, 2.531)
	$\rho$	2.079 (1.704, 2.384)
	$\bar{\nu}$	2.157 (1.899, 2.455)

Table A4: Marginal posterior estimates of initial viral (i.e. infectious 1st instar cadaver) densities, and of initial host density for C3-2015. Estimates are medians with 95% credible intervals. These are not on a log scale.

Parameter	Model (Informative Priors)	Estimate
	$\delta$	3.223 (1.314, 6.269)
	None	4.259 (2.354, 8.446)
	$C \rho \delta$	8.272 (3.173, 17.101)
P <sub>0</sub> , T1-2010	$C$	4.099 (1.972, 7.311)
	$C \rho \delta \bar{v}$	13.271 (4.126, 30.747)
	$\rho$	7.38 (2.498, 13.666)
	$\bar{v}$	19.551 (6.467, 45.627)
	$\delta$	0.01 (0.001, 0.041)
	None	0.02 (0, 0.105)
	$C \rho \delta$	0.052 (0.002, 0.216)
P <sub>0</sub> , T2-1987	$C$	0.029 (0, 0.159)
	$C \rho \delta \bar{v}$	0.152 (0.008, 0.698)
	$\rho$	0.065 (0.004, 0.477)
	$\bar{v}$	0.23 (0.005, 1.259)
	$\delta$	0.02 (0.004, 0.062)
	None	0.045 (0.006, 0.173)
	$C \rho \delta$	0.127 (0.003, 0.437)
P <sub>0</sub> , T3-1987	$C$	0.054 (0.015, 0.121)
	$C \rho \delta \bar{v}$	0.333 (0.086, 0.793)
	$\rho$	0.115 (0.029, 0.286)

	$\bar{\nu}$	0.538 (0.133, 1.227)
	$\delta$	0.018 (0.001, 0.057)
	None	0.026 (0.001, 0.159)
	$C \rho \delta$	0.075 (0.019, 0.171)
P <sub>0</sub> , T4-1987	$C$	0.044 (0.012, 0.095)
	$C \rho \delta \bar{\nu}$	0.221 (0.053, 0.519)
	$\rho$	0.091 (0.018, 0.261)
	$\bar{\nu}$	0.374 (0.085, 0.889)
	$\delta$	0.062 (0, 0.315)
	None	0.121 (0.027, 0.299)
	$C \rho \delta$	0.234 (0.014, 0.827)
P <sub>0</sub> , T5-1987	$C$	0.104 (0, 0.679)
	$C \rho \delta \bar{\nu}$	0.462 (0.072, 1.242)
	$\rho$	0.244 (0.031, 0.893)
	$\bar{\nu}$	0.724 (0.109, 2.1)
	$\delta$	47.855 (6.619, 148.114)
	None	49.627 (7.389, 124.164)
	$C \rho \delta$	47.754 (5.464, 134.17)
S <sub>0</sub> , C3-2015	$C$	51.902 (2.506, 179.48)
	$C \rho \delta \bar{\nu}$	62.45 (4.44, 171.538)
	$\rho$	41.987 (3.418, 133.317)
	$\bar{\nu}$	62.803 (10.467, 146.299)

Table A5: Marginal posterior estimates of transmission variability,  $\sigma_{e_t}$ , which is plot-specific. Estimates are medians with 95% credible intervals. These are not on a log scale.

Plot	Model	
	(Informative Priors)	Estimate
	$\delta$	2.742 (1.405, 5.048)
	None	3.546 (1.246, 6.572)
	$C \rho \delta$	4.293 (2.698, 6.609)
C1-2010	$C$	3.832 (1.893, 6.23)
	$C \rho \delta \bar{v}$	4.817 (3.393, 6.959)
	$\rho$	3.942 (2.033, 7.225)
	$\bar{v}$	5.641 (3.767, 7.924)
C2-1987	$\delta$	3.537 (0.337, 12.439)
	None	4.011 (2.165, 6.368)
	$C \rho \delta$	3.592 (0.758, 8.179)
	$C$	3.993 (0.74, 9.74)
	$C \rho \delta \bar{v}$	3.788 (0.646, 10.17)
	$\rho$	1.405 (0.132, 6.094)
	$\bar{v}$	2.705 (0.384, 7.888)
	$\delta$	0.769 (0.031, 3.865)
C3-2015	None	0.804 (0.006, 5.441)
	$C \rho \delta$	0.794 (0.02, 4.079)
	$C$	0.488 (0.001, 4.907)
	$C \rho \delta \bar{v}$	0.483 (0.001, 4.056)
	$\rho$	0.873 (0.02, 7.322)
	$\bar{v}$	0.5 (0.003, 3.693)
	$\delta$	3.636 (1.578, 6.299)

	None	2.597 (0.791, 6.158)
	$C \rho \delta$	1.959 (0.093, 9.11)
	$C$	2.858 (0.702, 6.928)
	$C \rho \delta \bar{\nu}$	1.86 (0.325, 5.442)
	$\rho$	1.535 (0.024, 6.543)
	$\bar{\nu}$	1.547 (0.048, 6.693)
<hr/>		
	$\delta$	0.111 (0.002, 0.754)
	None	0.117 (0.003, 0.775)
	$C \rho \delta$	0.099 (0, 0.866)
C5-2010	$C$	0.084 (0, 1.019)
	$C \rho \delta \bar{\nu}$	0.097 (0.001, 0.974)
	$\rho$	0.087 (0.001, 0.962)
	$\bar{\nu}$	0.052 (0, 0.717)
<hr/>		
	$\delta$	0.102 (0, 1.018)
	None	0.154 (0.002, 1.216)
	$C \rho \delta$	0.125 (0.001, 1.437)
C6-2010	$C$	0.098 (0.001, 0.914)
	$C \rho \delta \bar{\nu}$	0.128 (0, 1.453)
	$\rho$	0.202 (0.006, 1.162)
	$\bar{\nu}$	0.333 (0.012, 1.927)
<hr/>		
	$\delta$	0.095 (0.001, 0.937)
	None	0.222 (0.006, 1.261)
	$C \rho \delta$	0.098 (0, 1.443)
C7-1987	$C$	0.152 (0.006, 0.92)
	$C \rho \delta \bar{\nu}$	0.12 (0.002, 1.119)
	$\rho$	0.106 (0.001, 0.724)

	$\bar{\nu}$	0.136 (0.002, 0.796)
	$\delta$	0.368 (0.004, 2.743)
	None	0.352 (0.012, 1.921)
	$C \rho \delta$	0.41 (0.012, 2.487)
T1-2010	$C$	0.345 (0.002, 2.443)
	$C \rho \delta \bar{\nu}$	0.467 (0.003, 3.2)
	$\rho$	0.404 (0.003, 4.09)
	$\bar{\nu}$	0.21 (0, 2.63)
	$\delta$	2.976 (0.676, 7.66)
	None	2.896 (0.997, 6.441)
	$C \rho \delta$	3.499 (1.576, 6.053)
T2-1987	$C$	3.218 (0.166, 9.305)
	$C \rho \delta \bar{\nu}$	3.093 (1.504, 5.387)
	$\rho$	2.534 (0.829, 6.221)
	$\bar{\nu}$	2.92 (1.58, 4.817)
	$\delta$	0.294 (0.003, 2.722)
	None	0.237 (0.003, 3.072)
	$C \rho \delta$	0.571 (0.003, 4.353)
T3-1987	$C$	0.223 (0.001, 2.573)
	$C \rho \delta \bar{\nu}$	0.432 (0.002, 2.975)
	$\rho$	0.35 (0, 2.723)
	$\bar{\nu}$	0.359 (0.002, 2.113)
	$\delta$	0.105 (0, 1.598)
	None	0.105 (0.001, 1.194)
	$C \rho \delta$	0.363 (0.007, 2.03)
T4-1987	$C$	0.118 (0.001, 1.002)

	$C \rho \delta \bar{\nu}$	0.265 (0.001, 2.258)
	$\rho$	0.21 (0.004, 1.618)
	$\bar{\nu}$	0.16 (0.001, 1.936)
<hr/>		
	$\delta$	2.411 (0.008, 14.717)
	None	2.397 (0.066, 8.573)
	$C \rho \delta$	2.752 (0.15, 10.398)
T5-1987	$C$	2.966 (0.557, 7.488)
	$C \rho \delta \bar{\nu}$	2.56 (0.579, 6.598)
	$\rho$	2.325 (0.24, 6.59)
	$\bar{\nu}$	1.818 (0.071, 8.203)
<hr/>		

## 10 Marginal Posteriors For the $2-\bar{v}$ Models

Here we present tables with the marginal posterior parameter estimates derived from the  $2-\bar{v}$   
 405 models.

Table A6: Marginal posterior estimates of model parameters, where  $\gamma$  estimates the extra-binomial variation in fraction infected (see main text). Estimates are medians with 95% credible intervals. These are not on a log scale.

Parameter	Model (Informative Priors)	Estimate
$\delta$	$\delta$	0.064 (0.055, 0.073)
	$C \rho \delta$	0.064 (0.056, 0.073)
	None	0.062 (0.054, 0.074)
	$\bar{v}$ , TMB-1	0.073 (0.064, 0.083)
$C$	$\delta$	1.292 (1.084, 1.495)
	$C \rho \delta$	1.234 (1.135, 1.356)
	None	1.265 (1.078, 1.454)
	$\bar{v}$ , TMB-1	0.997 (0.815, 1.173)
$\mu$	$\delta$	0.016 (0, 0.183)
	$C \rho \delta$	0.044 (0.001, 0.188)
	None	0.048 (0, 0.374)
	$\bar{v}$ , TMB-1	0.011 (0, 0.069)
$\bar{v}$ , Control	$\delta$	0.067 (0.013, 0.191)
	$C \rho \delta$	0.049 (0.017, 0.101)
	None	0.073 (0.015, 0.233)
	$\bar{v}$ , TMB-1	0.026 (0.012, 0.046)

	$\delta$	0.252 (0.083, 0.718)
$\bar{v}$ , TMB-1	$C \rho \delta$	0.234 (0.079, 0.467)
	None	0.25 (0.077, 0.666)
	$\bar{v}$ , TMB-1	0.03 (0.013, 0.056)
<hr/>		
	$\delta$	0.018 (0.002, 0.058)
$\rho$	$C \rho \delta$	0.034 (0.011, 0.064)
	None	0.019 (0.002, 0.067)
	$\bar{v}$ , TMB-1	0.043 (0.016, 0.083)
<hr/>		
	$\delta$	2.124 (1.910, 2.386)
$\gamma$	$C \rho \delta$	2.25 (1.984, 2.517)
	None	2.059 (1.782, 2.335)
	$\bar{v}$ , TMB-1	2.214 (1.93, 2.517)

Table A7: Marginal posterior estimates of initial viral (i.e. infectious 1st instar cadaver) densities, and of initial host density for C3-2015. Estimates are medians with 95% credible intervals. These are not on a log scale.

Parameter	Model (Informative Priors)	Estimate
	$\delta$	3.187 (1.277, 6.944)
P <sub>0</sub> , T1-2010	$C \rho \delta$	3.222 (0.875, 6.576)
	None	3.687 (0.937, 9.667)
	$\bar{v}$ , TMB-1	9.946 (4.372, 17.728)
	$\delta$	0.009 (0, 0.057)
P <sub>0</sub> , T2-1987	$C \rho \delta$	0.015 (0, 0.09)
	None	0.02 (0.002, 0.066)
	$\bar{v}$ , TMB-1	0.117 (0.001, 0.622)
	$\delta$	0.017 (0.002, 0.057)
P <sub>0</sub> , T3-1987	$C \rho \delta$	0.027 (0.001, 0.111)
	None	0.028 (0.005, 0.068)
	$\bar{v}$ , TMB-1	0.254 (0.063, 0.626)
	$\delta$	0.013 (0.001, 0.053)
P <sub>0</sub> , T4-1987	$C \rho \delta$	0.019 (0.001, 0.088)
	None	0.016 (0.004, 0.047)
	$\bar{v}$ , TMB-1	0.177 (0.053, 0.376)
	$\delta$	0.069 (0.017, 0.146)
P <sub>0</sub> , T5-1987	$C \rho \delta$	0.069 (0.008, 0.204)
	None	0.086 (0.01, 0.235)
	$\bar{v}$ , TMB-1	0.401 (0.078, 1.146)
	$\delta$	72.375 (15.566, 169.075)

$C \rho \delta$	68.895 (12.593, 172.337)
None	71.492 (9.571, 219.717)
$\bar{\nu}$ , TMB-1	53.987 (23.135, 98.69)

---

Table A8: Marginal posterior estimates of transmission variability,  $\sigma_{e_t}$ , which is plot-specific. Estimates are medians with 95% credible intervals. These are not on a log scale.

Plot	Model	
	(Informative Priors)	Estimate
	$\delta$	4.564 (1.488, 8.99)
C1-2010	$C \rho \delta$	5.259 (3.282, 7.162)
	None	4.625 (1.65, 7.774)
	$\bar{v}$ , TMB-1	4.871 (3.271, 6.792)
C2-1987	$\delta$	3.016 (0.997, 7.627)
	$C \rho \delta$	3.399 (0.618, 8.782)
	None	3.362 (0.074, 18.944)
C3-2015	$\bar{v}$ , TMB-1	2.623 (0.045, 14.099)
	$\delta$	0.616 (0.018, 3.576)
	$C \rho \delta$	0.454 (0.001, 4.425)
C4-1987	None	0.511 (0.004, 3.609)
	$\bar{v}$ , TMB-1	0.499 (0, 4.605)
	$\delta$	2.989 (1.188, 5.574)
C5-2010	$C \rho \delta$	2.181 (0.139, 7.823)
	None	2.577 (0.435, 5.734)
	$\bar{v}$ , TMB-1	2.645 (0.346, 6.965)
C6-2010	$\delta$	0.127 (0, 1.514)
	$C \rho \delta$	0.138 (0.002, 1.454)
	None	0.259 (0.007, 1.526)
	$\bar{v}$ , TMB-1	0.067 (0, 0.964)
	$\delta$	0.261 (0.001, 2.125)
	$C \rho \delta$	0.286 (0.001, 2.04)

	None	0.305 (0.001, 2.783)
	$\bar{\nu}$ , TMB-1	0.225 (0.003, 1.784)
	$\delta$	0.172 (0.005, 1.268)
C7-1987	$C \rho \delta$	0.109 (0, 1.728)
	None	0.163 (0.008, 1.358)
	$\bar{\nu}$ , TMB-1	0.078 (0, 1.034)
	$\delta$	0.195 (0.002, 1.804)
T1-2010	$C \rho \delta$	0.19 (0, 2.471)
	None	0.363 (0.003, 3.082)
	$\bar{\nu}$ , TMB-1	0.268 (0, 3.593)
	$\delta$	1.745 (0.064, 6.314)
T2-1987	$C \rho \delta$	1.599 (0.003, 8.071)
	None	1.536 (0.047, 6.791)
	$\bar{\nu}$ , TMB-1	3.324 (1.505, 6.18)
	$\delta$	0.213 (0.001, 2.038)
T3-1987	$C \rho \delta$	0.139 (0, 2.433)
	None	0.25 (0.001, 2.396)
	$\bar{\nu}$ , TMB-1	0.446 (0.006, 2.844)
	$\delta$	0.111 (0.001, 1.253)
T4-1987	$C \rho \delta$	0.066 (0, 1.211)
	None	0.088 (0.001, 1.059)
	$\bar{\nu}$ , TMB-1	0.173 (0.002, 1.271)
	$\delta$	1.392 (0.067, 6.406)
T5-1987	$C \rho \delta$	2.174 (0.068, 8.63)
	None	1.588 (0.103, 6.538)
	$\bar{\nu}$ , TMB-1	2.679 (0.272, 8.737)

## 11 Visual fits to the observational data for each of the $1-\bar{v}$ models.

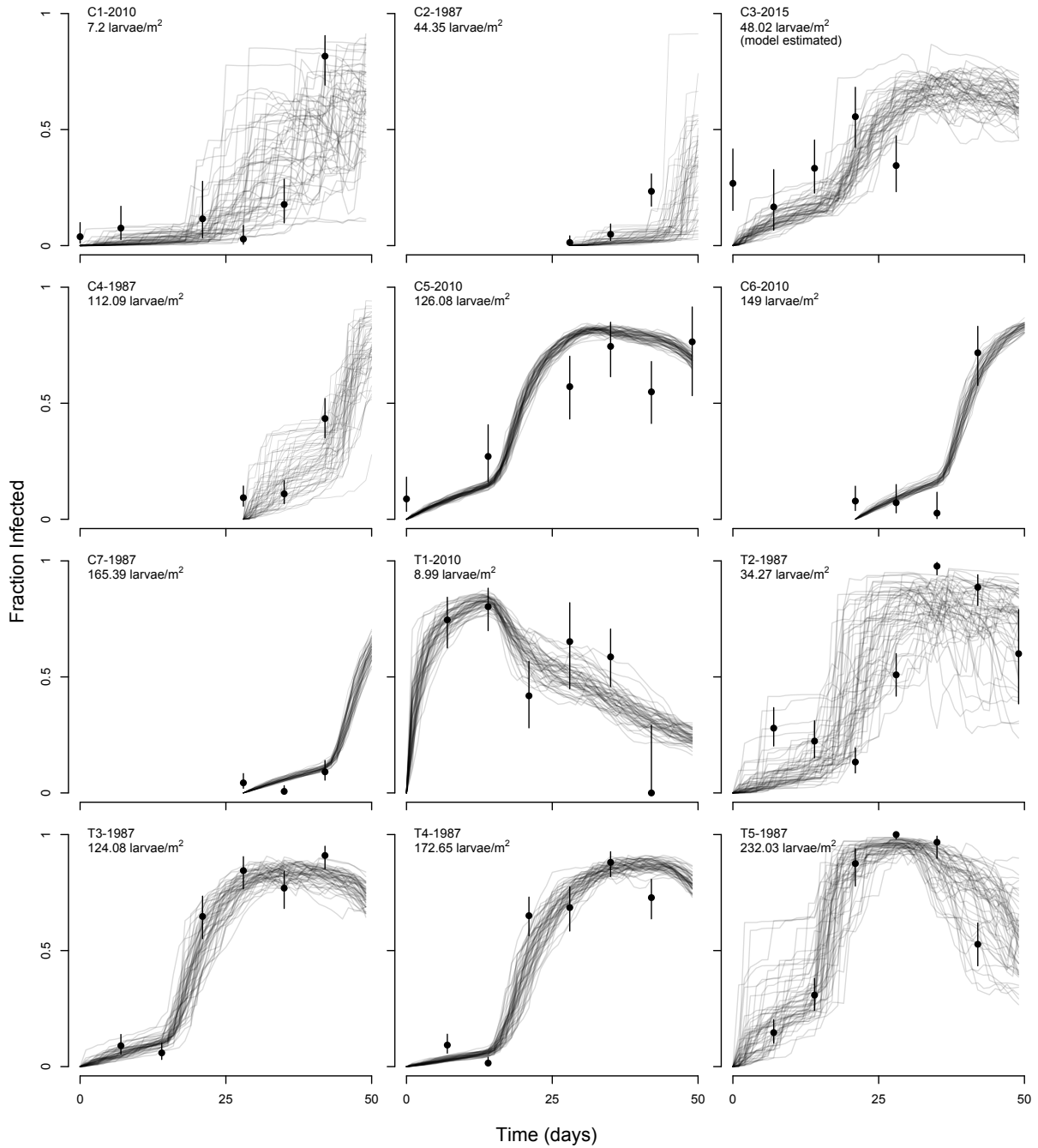


Figure A9: Stochastic realizations of the model that has experiment-based priors on the transmission heterogeneity parameter  $C$ , the ratio parameter  $\rho$ , and the death rate  $\delta$ .

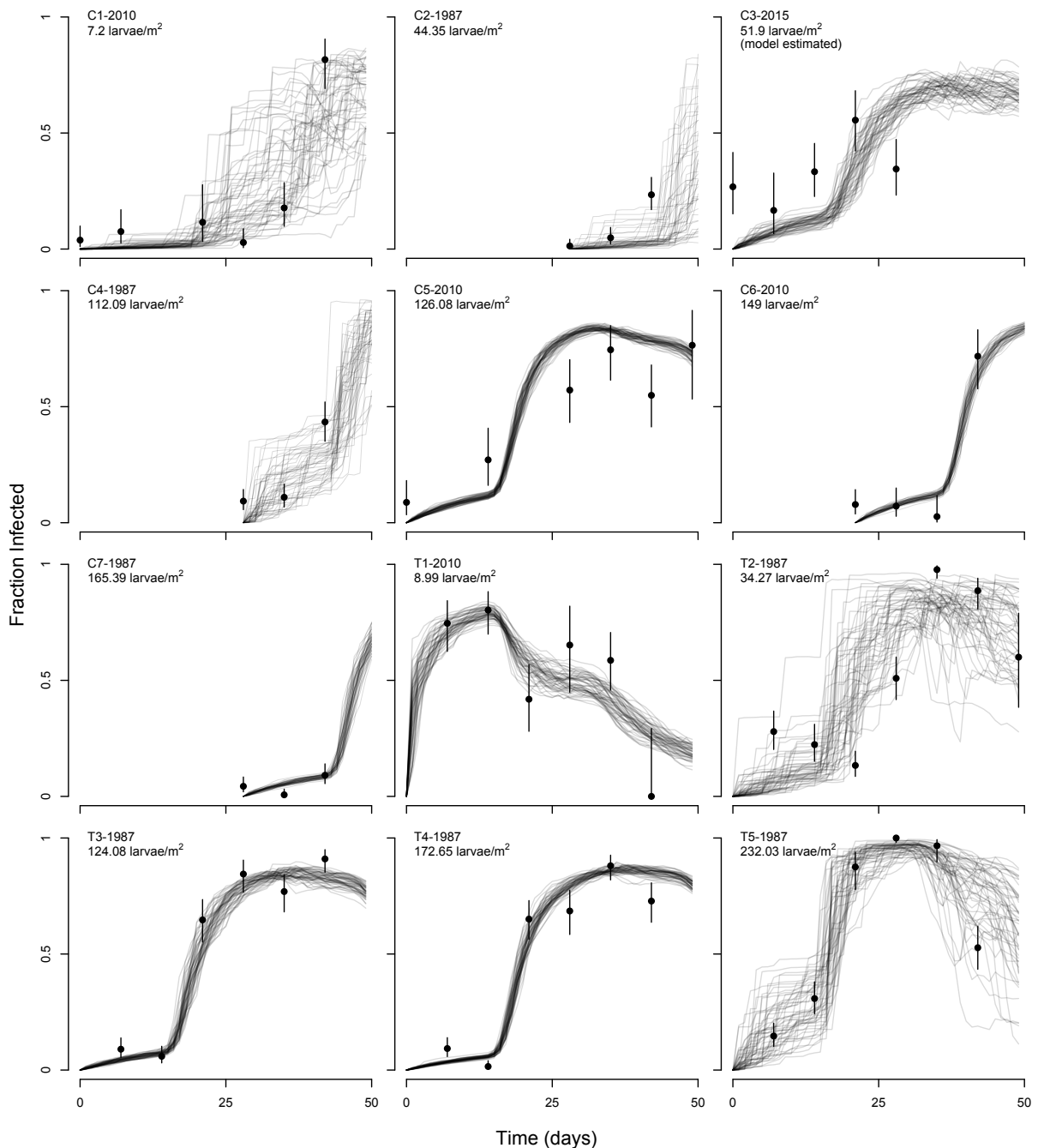


Figure A10: Stochastic realizations of the model that has an experiment-based prior on the transmission heterogeneity parameter  $C$ .

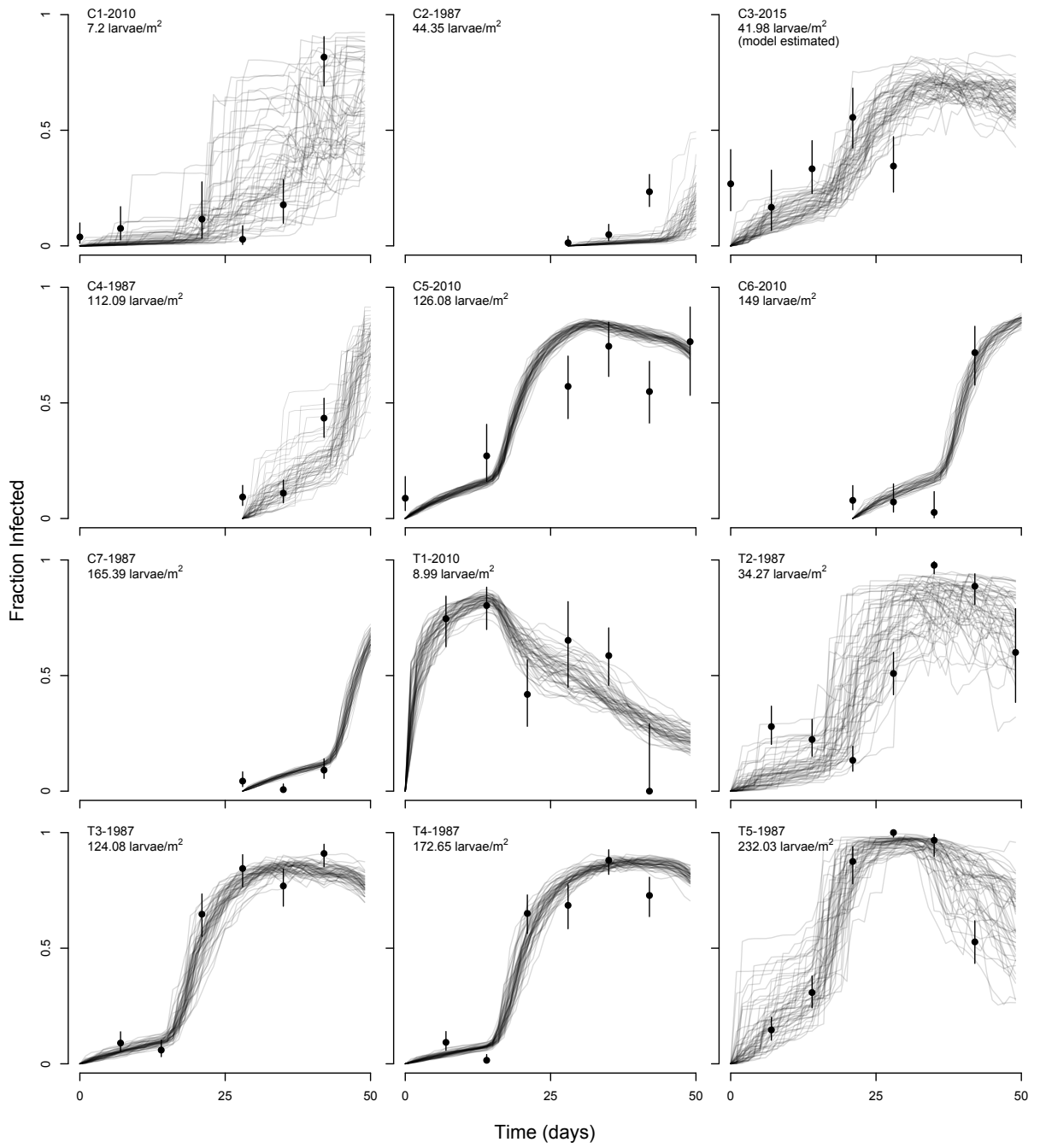


Figure A11: Stochastic realizations of the model that has an experiment-based prior on the ratio parameter  $\rho$ .

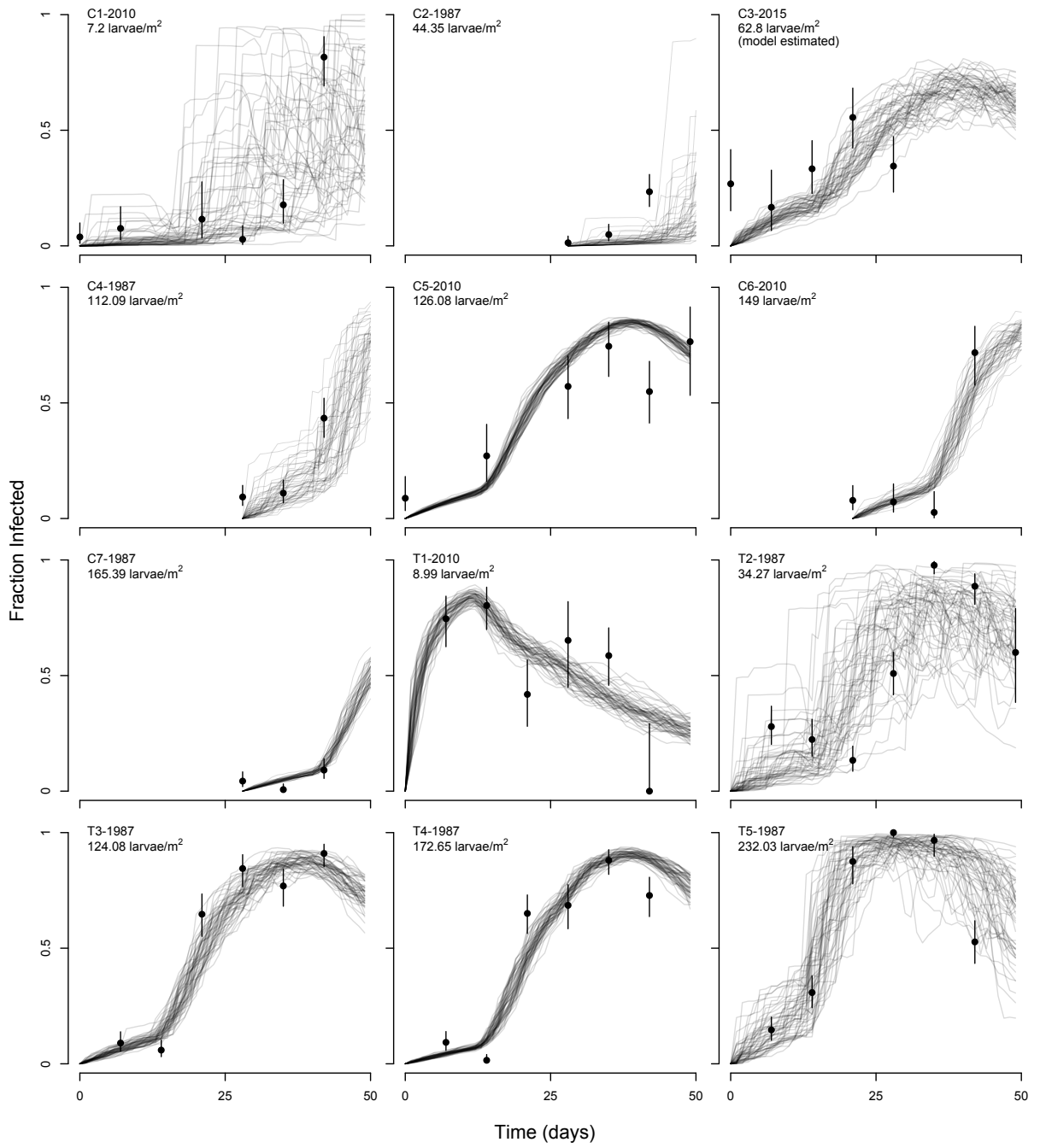


Figure A12: Stochastic realizations of the model that has an informative prior on the average transmission parameter  $\bar{v}$ .

## 12 Visual fits to the observational data for each of the $2-\bar{v}$ models.

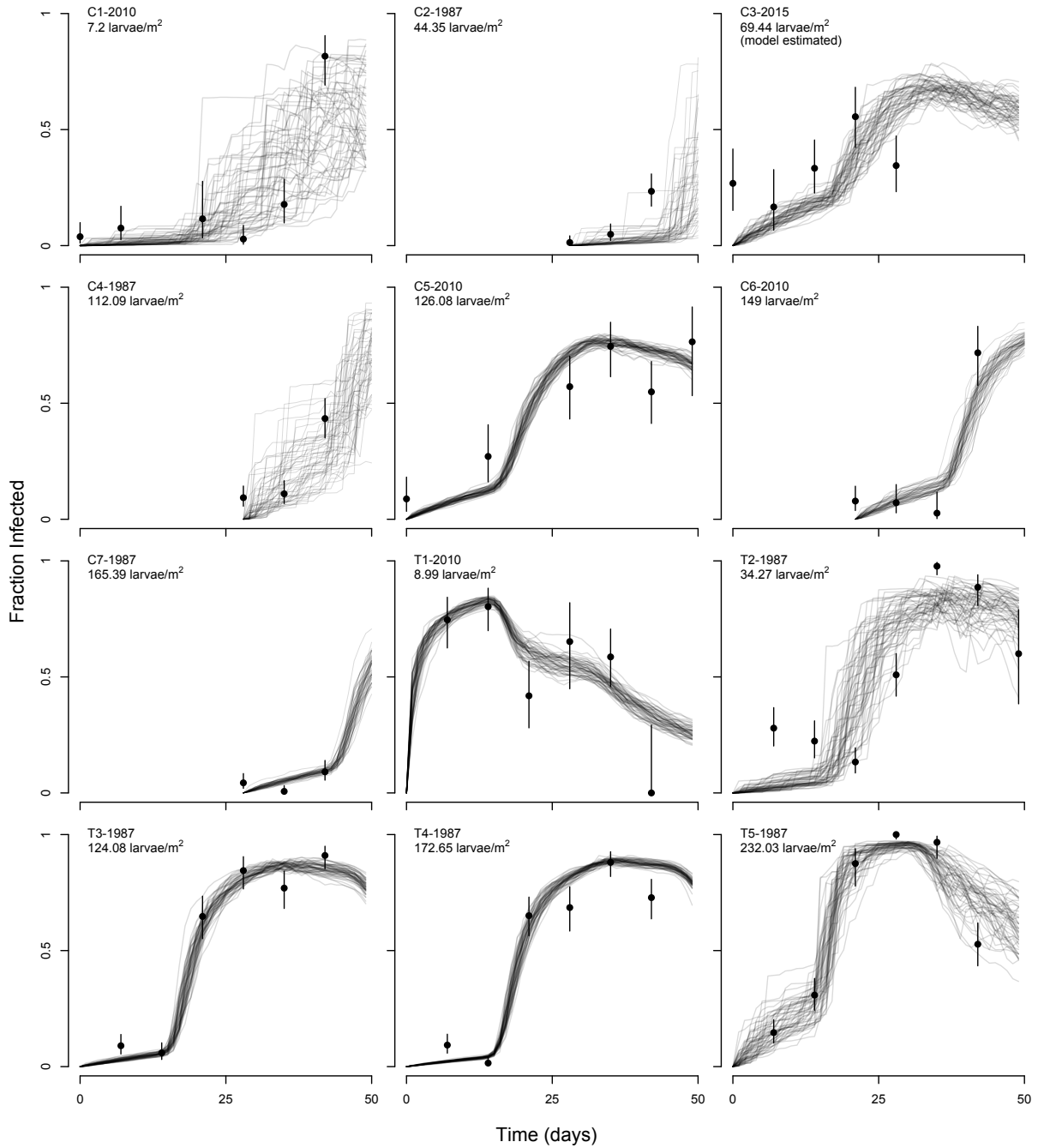


Figure A13: Stochastic realizations of the  $2-\bar{v}$  model that has an informative prior on the death rate parameter  $\delta$ .

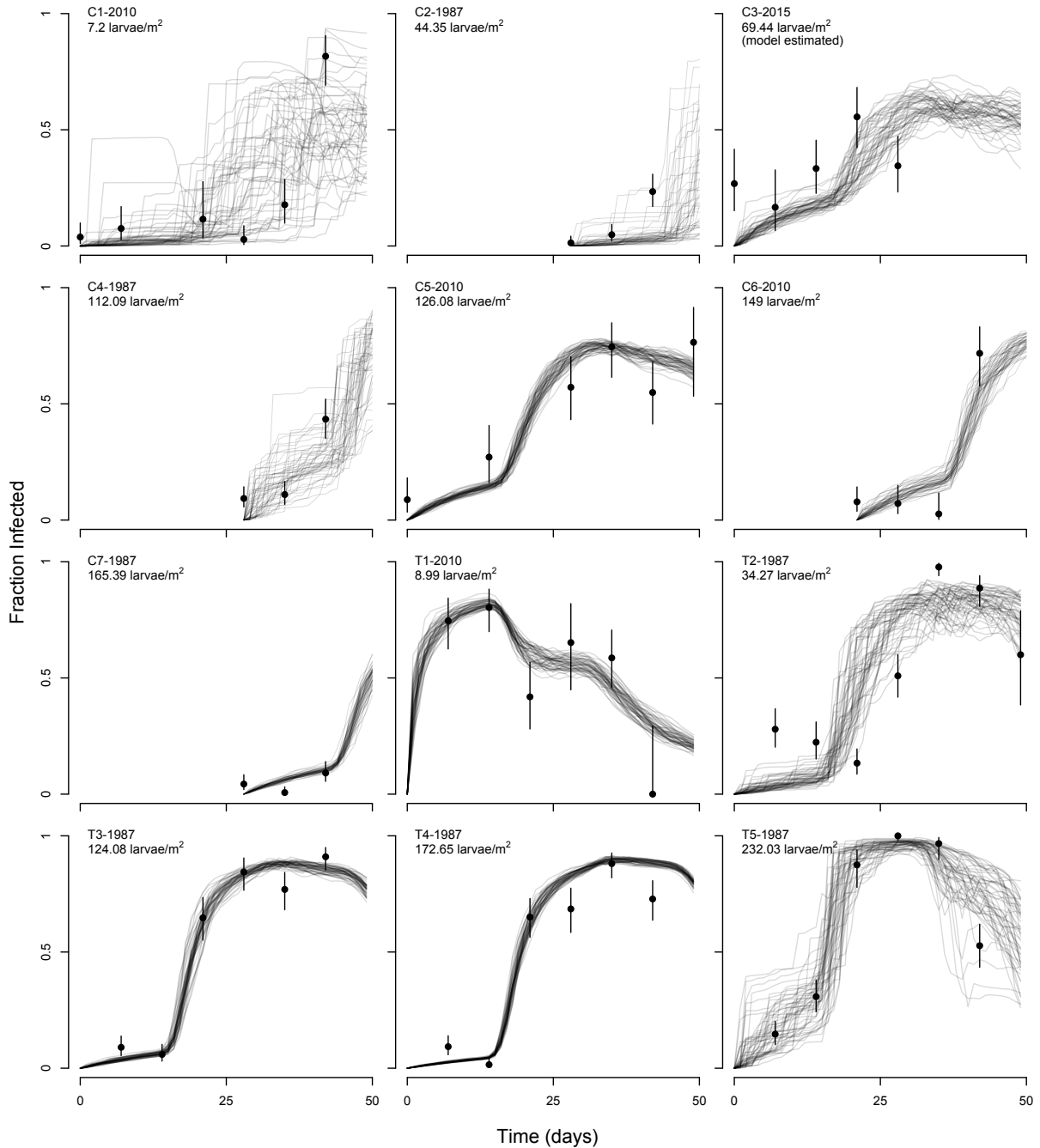


Figure A14: Stochastic realizations of the  $2-\bar{v}$  model that has experiment-based priors on the heterogeneity parameter  $C$ , the ratio parameter  $\rho$ , and the mortality parameter  $\delta$ .

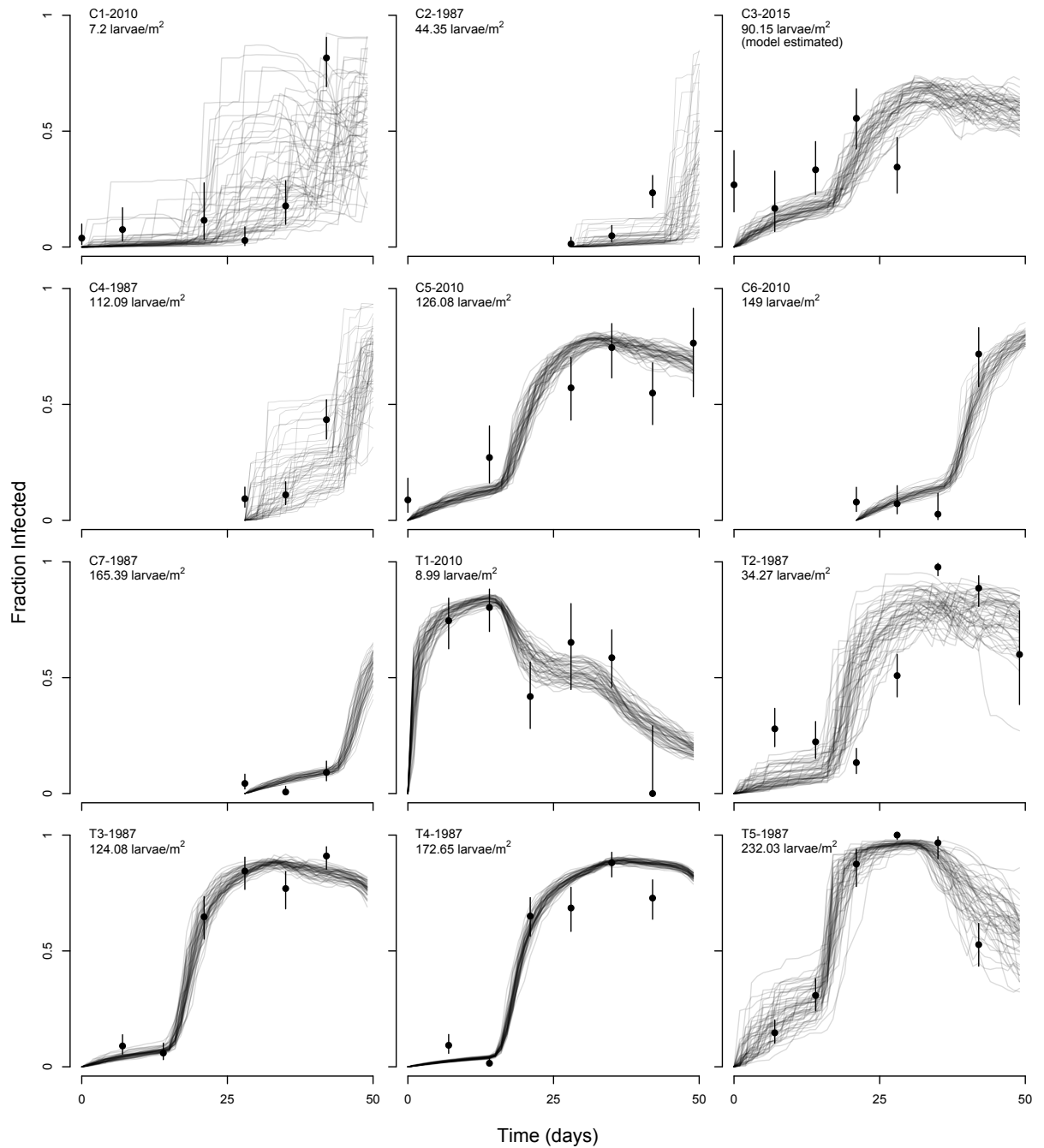


Figure A15: Stochastic realizations of the  $2-\bar{v}$  model that has only uninformative priors.

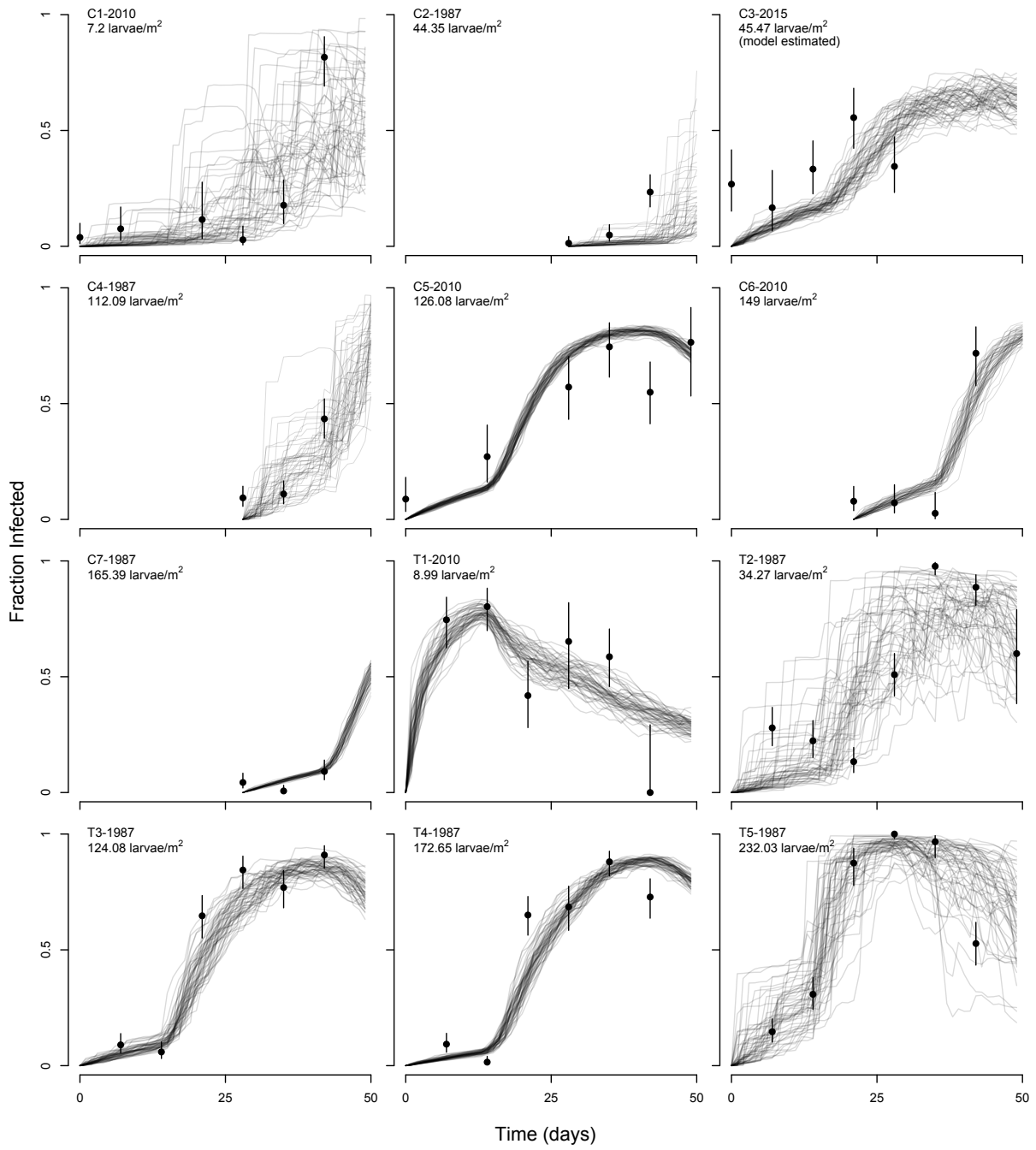


Figure A16: Stochastic realizations of the  $2-\bar{v}$  model that has an informative prior on the sprayed (TMB-1) virus' average transmission rate,  $\bar{v}_{TMB-1}$ .

## 13 JAGS model statement for fitting the transmission model to experimental data

```

model{

#####
# Priors #
#####

# Virus-level transmission parameters.
# Three viruses: TMB-1, WA, NM

for(v in 1:3){

  # C and nu.bar (log scale):
  nC[v] ~ dnorm(0, 1 / (1 ^ 2))
  nnu.bar[v] ~ dnorm(-8, 1 / (2 ^ 2))

  C[v] <- exp(nC[v])
  nu.bar[v] <- exp(nnu.bar[v])
}

# Error in Initial Cadaver Density:
# Error in cadaver density varies by experimental treatment.
# (i.e. 1, 2, 3 represent 0, 10, or 40 initial cadavers)

for(d in 1:3){

  p.mean[d] ~ dnorm(0, .001)
}
}

```

```

p.sd[d] ~ dgamma(0.001,0.001)
p.tau[d] <- 1 / (p.sd[d])^2
}

# Ratio parameter:

# Informative prior generated by counting virus in
# first and fourth instar larvae

nratio ~ dnorm(-3.387, 1 / 0.25^2)
ratio <- exp(nratio)

#####
# LIKELIHOOD #
#####

for(i in 1:N.obs){

  # Binomial likelihood:
  # n.inf = number infected from each bag
  # n.recov = total number recovered from each bag at end of experiment

  n.inf[i] ~ dbin(prob[i], n.recov[i])

  # Heterogeneity model:

  prob[i] <- 1 - (1 + (C[Virus[i]])^2 * nu.bar[Virus[i]] *
    (P[i]+0.00001) * ratio * 7)^(-1/(C[Virus[i]]^2))
}

}

```

```

#####
# ERROR IN CAD. DENSITY #
#####

# P = estimated cadaver density,
# based on estimated area of foliage in each bag
# Cad.Den = vector of treatment identifiers
# (i.e. 1, 2, 3 represent 0, 10, or 40 initial cadavers)

for(i in 1:N.obs){
  P[i] ~ dnorm(p.mean[Cad.Den[i]], p.tau[Cad.Den[i]])
}

}

```

## 14 JAGS model statement to fit a Gamma distribution to the time-to-death data

```
model{

#####  
# Priors #  
#####  
  
g_alpha ~ dunif(0, 100)  
g_beta ~ dunif(0, 100)  
  
#####  
# LIKELIHOOD #  
#####  
# y = vector with time-to-death for each larva  
  
for(i in 1:n_samp){  
    y[i] ~ dgamma(g_alpha, g_beta)  
}  
  
}
```

## Literature Cited

- 411 Bolker, B. M. 2008. Ecological models and data in R. Princeton University Press.
- D'Amico, V., J. S. Elkinton, J. D. Podgwaite, J. Buonaccorsi, and G. Dwyer. 2005. Pathogen  
clumping: an explanation for non-linear transmission of an insect virus. *Ecological Entomology*  
414 30:383–390.
- Dwyer, G. 1991. The effects of density, stage and spatial heterogeneity on the transmission of an  
insect virus. *Ecology* 72:559–574.
- 417 ———. 1992. On the spatial spread of insect pathogens - theory and experiment. *Ecology* 73:479–  
494.
- Dwyer, G., and J. S. Elkinton. 1995. Host dispersal and the spatial spread of insect pathogens.  
420 *Ecology* 76:1262–1275.
- Dwyer, G., J. S. Elkinton, and J. P. Buonaccorsi. 1997. Host heterogeneity in susceptibility and  
disease dynamics: Tests of a mathematical model. *American Naturalist* 150:685–707.
- 423 Dwyer, G., J. Firestone, and T. E. Stevens. 2005. Should models of disease dynamics in herbivorous  
insects include the effects of variability in host-plant foliage quality? *American Naturalist*  
165:16–31.
- 426 Eakin, L., M. Wang, and G. Dwyer. 2015. The effects of the avoidance of infectious hosts on  
infection risk in an insect-pathogen interaction. *Am. Nat.* 185:pp. 100–112.
- Elderd, B. D., J. Dushoff, and G. Dwyer. 2008. Host-pathogen interactions, insect outbreaks, and  
429 natural selection for disease resistance. *The American Naturalist* 172:829–842.
- Fleming-Davies, A. E., V. Dukic, V. Andreasen, and G. Dwyer. 2015. Effects of host heterogeneity  
on pathogen diversity and evolution. *Ecology Letters* 18:1252–1261.

- 432 Fuller, E., B. D. Elderd, and G. Dwyer. 2012. Pathogen persistence in the environment and insect-baculovirus interactions: Disease-density thresholds, epidemic burnout, and insect outbreaks. Am. Nat. 179:pp. E70–E96.
- 435 Gelman, A., J. B. Carlin, H. S. Stern, D. B. Dunson, A. Vehtari, and D. B. Rubin. 2014. Bayesian Data Analysis, Third Edition. Chapman & Hall/CRC Press. New York, NY.
- Grove, M. J., and K. Hoover. 2007. Intrastadial developmental resistance of third instar gypsy moths (*Lymantria dispar* l.) to *L. dispar* nucleopolyhedrovirus. Biological Control 40:355–361.
- 438 Hughes, K., and R. Addison. 1970. Two nuclear polyhedrosis viruses of Douglas-fir tussock moth. Journal of Invertebrate Pathology 16:196–&.
- 441 Kennedy, D. A., V. Dukic, and G. Dwyer. 2014. Pathogen Growth in Insect Hosts: Inferring the Importance of Different Mechanisms Using Stochastic Models and Response-Time Data. American Naturalist 184:407–423.
- 444 Kernighan, B. W., and D. M. Ritchie. 2006. The C programming language.
- Konishi, S., and G. Kitagawa. 2008. Information criteria and statistical modeling. Springer Science & Business Media.
- 447 Mason, R., D. Scott, and H. Paul. 1993. Forecasting Outbreaks of the Douglas-Fir Tussock Moth From Lower Crown Cocoon Samples. USDA Forest Service Research Paper PNW-RP-460.
- Mason, R., and T. Torgersen. 1983. Mortality of larvae in stocked cohorts of the Douglas-fir tussock moth, *Orgyia pseudotsugata* (Lepidoptera: Lymantriidae). Canadian Entomologist 115:1119–1127.
- 450 Mason, R. R., R. Beckwith, and H. G. Paul. 1977. Fecundity Reduction During Collapse of a Douglas-fir Tussock Moth Outbreak in Northeast Oregon. Environmental Entomology 6:623–626.

- Otvos, I. S., J. C. Cunningham, and L. M. Friskie. 1987. Aerial application of nuclear polyhedrosis virus against douglas-fir tussock moth, *Orgyia pseudostugata* (Mcdunnough) (Lepidoptera: Lymantriidae). 1. impact in the year of application. Canadian Entomologist 119:697–706.
- Páez, D., V. Dukic, J. Dushoff, A. Fleming-Davies, and G. Dwyer. 2017. Effects of pathogen exposure on life-history variation in the gypsy moth (lymantria dispar). The American Naturalist accepted pending minor revision.
- Parker, B. J., B. D. Elderd, and G. Dwyer. 2010. Host behaviour and exposure risk in an insect-pathogen interaction. Journal of Animal Ecology 79:863–870.
- Press, W. H., S. A. Teukolsky, W. T. Vetterling, and B. P. Flannery. 1992. Numerical recipes in C, vol. 2. Cambridge university press Cambridge.
- Ross, S. 2002. Simulation, 3rd. Edition. Academic Press, New York.
- Schindelin, J., C. T. Rueden, M. C. Hiner, and K. W. Eliceiri. 2015. The ImageJ ecosystem: An open platform for biomedical image analysis. Molecular Reproduction and Development 82:518–529.
- Stelzer, R. 1979. How to determine the incidence of virus in egg masses. Douglas-fir tussock moth handbook. USDA agriculture handbook .
- Watanabe, S. 2009. Algebraic geometry and statistical learning theory, vol. 25. Cambridge University Press.